AD NUMBER

AD847001

LIMITATION CHANGES

TO:

Approved for public release; distribution is unlimited.

FROM:

Distribution authorized to U.S. Gov't. agencies and their contractors; Critical Technology; OCT 1968. Other requests shall be referred to Office of Naval Research, Code 421, Washington, DC 20360. This document contains export-controlled technical data.

AUTHORITY

onr notice, 27 jul 1971

ADVANCED CAPABILITY INFRARED RECEIVER SYSTEM

FIRST SEMIANNUAL PROGRESS REPORT
(15 March 1968 to 15 September 1968)

October 1968

by

F. Pace, F. Arams, R. Lange, B. Peyton, E. Sard and, J. Ramsey

AIL Report 3481-I-1
Prepared Under Contract N00014-68-C-0273
ARPA Order No. 306
Project Code 7E20K21
for
Office of Naval Research
Washington, D.C.

by

AIRBORNE INSTRUMENTS LABORATORY
A DIVISION OF CUTLER-HAMMER, INC.
Deer Park, New York 11729

This research is part of Project DEFENDER under the joint sponsorship of the Advanced Research Projects Agency, the Office of Naval Research, and the Department of Defense. Reproduction in whole, or in part, is permitted for any purpose of the United States Government.

ADVANCED CAPABILITY INFRARED RECEIVER SYSTEM

FIRST SEMIANNUAL PROGRESS REPORT
(15 March 1968 to 15 September 1968)

October 1968

by

F. Pace, F. Arams, R. Lange, B. Peyton, E. Sard and, J. Ramsey

AIL Report 3481-I-1
Prepared Under Contract N00014-68-C-0273
ARPA Order No. 306
Project Code 7E20K21
for
Office of Naval Research
Washington, D. C.

by

AIRBORNE INSTRUMENTS LABORATORY
A DIVISION OF CUTLER-HAMMER, INC.
Deer Park, New York 11729

This research is part of Project DEFENDER under the joint sponsorship of the Advanced Research Projects Agency, the Office of Naval Research, and the Department of Defense. Reproduction in whole, or in part, is permitted for any purpose of the United States Government.

ACKNOWLEDGMENT

The authors gratefully acknowledge the technical contributions of A. DiNardo, A. Faveiro, and Dr. S. Rosin (Consultant).

TABLE OF CONTENTS

BLANK PAGE

LIST OF ILLUSTRATIONS

I. INTRODUCTION AND SUMMARY

This is the first semiannual progress report on a program having as its objective the feasibility demonstration of an infrared 10.6-micron coherent receiver array with a 1.5-GHz wideband IF capability, 3 × 3 elements with -3 db antenna-beam crossovers, and near-theoretical quantum-noise limited sensitivity performance.

The first six months of the program, 15 March 1968 to 15 September 1968 (with reduced level until the executed contract was received on 4 June 1968), has been directed toward obtaining by analysis, experimentation, and study the data required for synthesizing several possible approaches and selecting the one or two approaches that are most likely to yield a feasible coherent array with the required performance characteristics. The balance of this program will demonstrate that the selected approach is truly feasible in practice and that the objective specifications can be met.

Two primary areas of investigation were identified:

- Coherent array development,
- Mixer development.

The coherent array development includes the optical, mechanical, and electrical problems associated with such mixer element parameters as size and spacing, and the method of achieving the multielement beam patterns and -3 db crossovers. The mixer development concerns itself with the mixer materials, properties, and electronics, and optimizing them to obtain sensitivities near the quantum-noise limit, in combination with 1.5 GHz instantaneous bandwidth.

The investigation of these two areas was based on technical guidelines established by earlier work on 10.6-micron mixer elements (references 1 and 2). The findings are summarized and reported in the sections that follow. The integration and application of these findings will give what promises to be a feasible coherent wideband two-dimensional array technology.

A. COHERENT ARRAY DEVELOPMENT

An analytical model has been formulated for a coherent multiple-beam array. Computer calculations on optimum illumination patterns and mixer geometry to yield high signal-conversion efficiencies and controlled beam crossovers have been completed. The computed patterns indicate the range of mixer and optical parameters for which -3 db beam crossovers may be efficiently achieved.

An optical beam pattern test range has been set up in the laboratory and the patterns obtained agree well with the computed patterns.

Several approaches have been investigated for dissecting the diffraction-limited spot in the image plane. This is a key problem in the array fabrication. The most promising are: (1) multifaceted wedges, and (2) microlenses with integrated-circuit mixer elements. Detailed optical designs are being carried out.

B. 10.6-MICRON COHERENT MIXER DEVELOPMENT

For high-frequency response, mixing was obtained with response extended to 1.43 GHz (instantaneous frequency response 10 MHz to 1.43 GHz) using an improved Ge:Cu mixer/low-noise amplifier combination. Measurements indicate a noise equivalent power of 1.5×10^{-19} watt/Hz, or less, over this complete band.

An analysis on high-frequency photovoltaic mixing was completed, and specifications for a PV mixer were written. Broadbanding, using maximally flat double and triple tuning, was also investigated.

Measurements on high frequency response, and mixer sensitivity, of various mixer elements including Ge:Cu, Ge:Hg, Si:Al, and higher-temperature HgCdTe, are reported.

II. COHERENT ARRAY DEVELOPMENT

A. OPTICAL PATTERN SYNTHESIS

Synthesizing the far-field diffraction pattern for a coherent optical array involves a departure from long-wavelength antenna procedures in that the optical array pattern is strongly affected by the phase-front of the reference or local oscillator beam, which must be included in the design. The array design requires nine identical signal beams, squinted with respect to one another, with crossovers at -3 db points, between adjacent beams.

The approach chosen, to achieve such an overall pattern, was to design the local oscillator beam to be a plane wave traveling normal to the plane of the array and uniformly irradiating it. This approach also has the virtue of simplifying the receiver optics. The signal beam shapes are then found to be fixed by the diffraction field associated with the limiting aperture of the incoming signal optics.

Figure 2-1 illustrates this situation. The receiving optics transform wavefront tilt of the signal radiation in the receiving aperture into translation about the optic axis in the image plane. This focused signal is added to the plane-wave (approximate) local oscillator in the image plane.

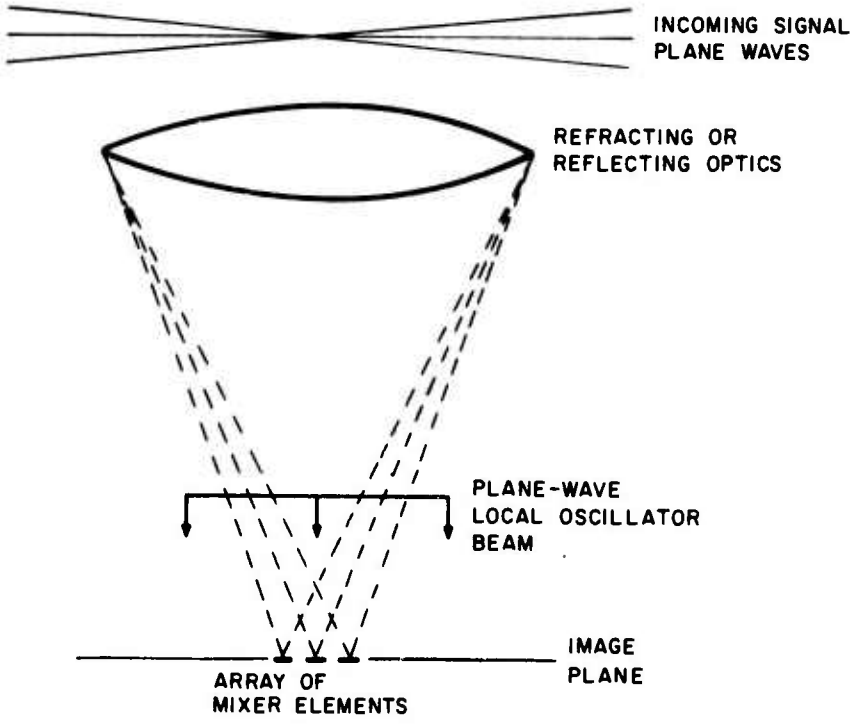

FIGURE 2-1. DIAGRAM OF BEAM-FORMING OPTICS

In the process of photomixing, the product of the field vectors, representing the local oscillator and the received signal, is obtained at the mixer and their resultant is detected. The combined envelope may be viewed as an extension of the classical interference pattern. To interfere efficiently, the polarization of the two components must be aligned. In the discussion that follows, it is assumed that this requirement is fulfilled. To linearize the mixing process, the local oscillator amplitude is made orders-of-magnitude greater than that of the received signal. Since there is likely to be a frequency offset between the two mixed components, the fringes are not static but oscillate rapidly at the difference frequency. Expressions are now derived for the complex amplitudes (electric fields) of the received signal and the local oscillator at the image plane, for it is here that the mixer element is placed to detect the dynamic interference fringes.

Consider, first, the received signal that is focused by the receiving aperture onto the image plane within the coordinate system defined in Figure 2-2. The incoming signal propagates in the direction given by:

$$\bar{n} = \bar{i}\alpha' + \bar{j}\beta' + \bar{k}\gamma'$$

where

$\bar{i}$, $\bar{j}$, $\bar{k}$ = unit vectors for the rectangular coordinate system

α', β', γ' = direction cosines, and any point in the aperture plane is

$$\bar{r} = \bar{i}\xi + \bar{j}\eta$$

where ξ, η = aperture plane coordinates.

Under certain conditions, the field at the receiving aperture is related to the field at the image plane by the Fourier transformation. The expression for this transformation is derived by Silver (reference 3) and Stroke (reference 4). According to Stroke, three important approximations to the vigorous electromagnetic wave treatment of this field vector problem are involved in the derivation of the Fourier integral representation of the Fraunhofer region. This representation applies to:

1. Center and near-vicinity of a quasi-spherical wavefront of radius R
2. Values of wavelength $\lambda \ll R$
3. a) Electromagnetic field vectors $\bar{E}$ and $\bar{H}$ which are tangent to the wavefront, and
   b) $\bar{E}$, $\bar{H}$, and the gradient of the wavefront, which form an orthogonal triad

Condition 1 refers to that region where small angle approximations are valid; that is, the case of interest here. Condition 2 is certainly met at infrared wavelengths. Conditions 3 and 4 are met for high f/number systems in that, in such a case, the bundle of rays converges slowly to a focus. It has been shown (references 5 and 6) that an f/number greater than four ensures the validity of the scalar approximation of the vector treatment of electromagnetic wave interactions at the focus of a lens.

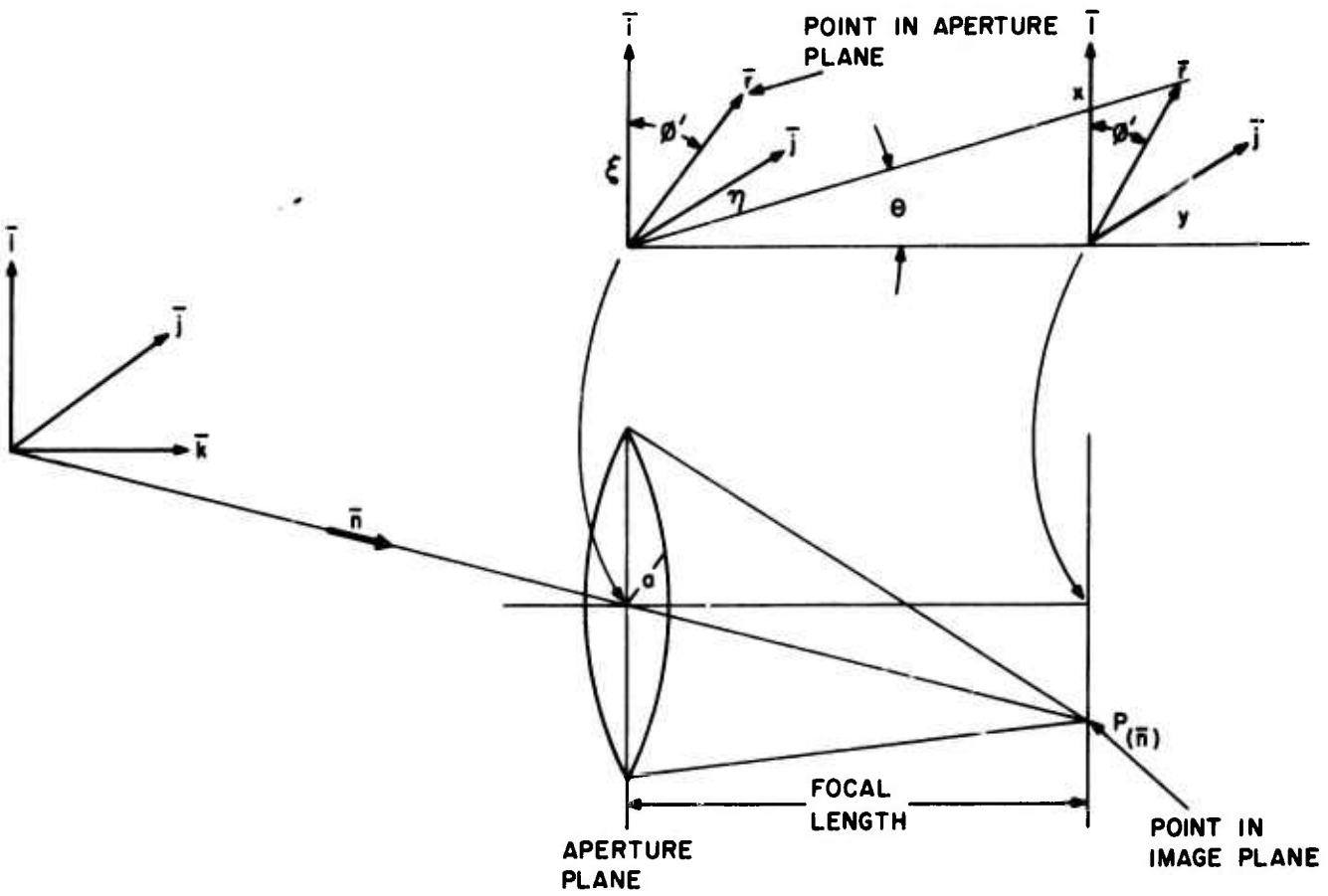

FIGURE 2-2. COORDINATES FOR HETERODYNE RECEIVER BEAM PATTERN ANALYSIS

Stroke's formulation of the Fourier integral representation is given as:

$$\bar{E}_p(k\alpha,\ k\beta) = \frac{i}{\lambda}\,\frac{e^{-ikf}}{f} \int_{\substack{\xi \\ \text{aperture} \\ \text{plane}}} \int_{\eta} \bar{E}_o\ e^{ik\Delta(\xi,\,\eta)}\ e^{ik(\alpha\xi\,+\,\beta\eta)}\ d\xi d\eta$$

where

$\bar{E}_p(k\alpha,\ k\beta)$ = complex amplitude of the electric field vector at a point (P), in the image plane, with coordinate values $(k\alpha,\ k\beta)$

$k = 2\pi/\lambda$

λ = wavelength

$(k\alpha,\ k\beta)$ = image plane coordinates expressed in terms of the direction cosines of plane waves incident on the receiving aperture

$i = \sqrt{-1}$

f = focal length of lens

(ξ, η) = rectangular coordinates of aperture plane

$\bar{E}_o = E_T e^{-i\omega_T t}$ = complex amplitude of the electric field, in the aperture plane, with sinusoidal time variation ω_T

The phase variation over the aperture, with respect to the coordinate origin, is given by:

$$\Delta = k\,\bar{r} \cdot \bar{n} = k(\xi\alpha' + \eta\beta')$$

For the paraxial case, where $\bar{n}$ is at only small angles to the optic axis:

$$\alpha' \cong \frac{x'}{f} \text{ and } \beta' \cong \frac{y'}{f}$$

likewise

$$\alpha \cong \frac{x}{f} \text{ and } \beta \cong \frac{y}{f}$$

For a uniform plane wave incident from direction $\bar{n}$, E_T is constant and Δ is as given. This reduces the integral to the form:

$$I_o = \int_\xi \int_\eta e^{i\frac{k}{f}\left[(x + x')\,\xi + (y + y')\beta\right]} d\xi\, d\eta$$

For a circular aperture let

$$\xi = \rho \cos \phi'$$

$$\eta = \rho \sin \phi'$$

$$\rho = \left(\xi^2 + \eta^2\right)^{1/2}$$

where ϕ' is defined in Figure 2-2. With this substitution

$$I_o = \int_0^a \int_0^{2\pi} e^{\frac{ik\rho}{f}\left[(x + x')\cos\phi' + (y + y')\sin\phi'\right]} \rho\, d\phi'\, d\rho$$

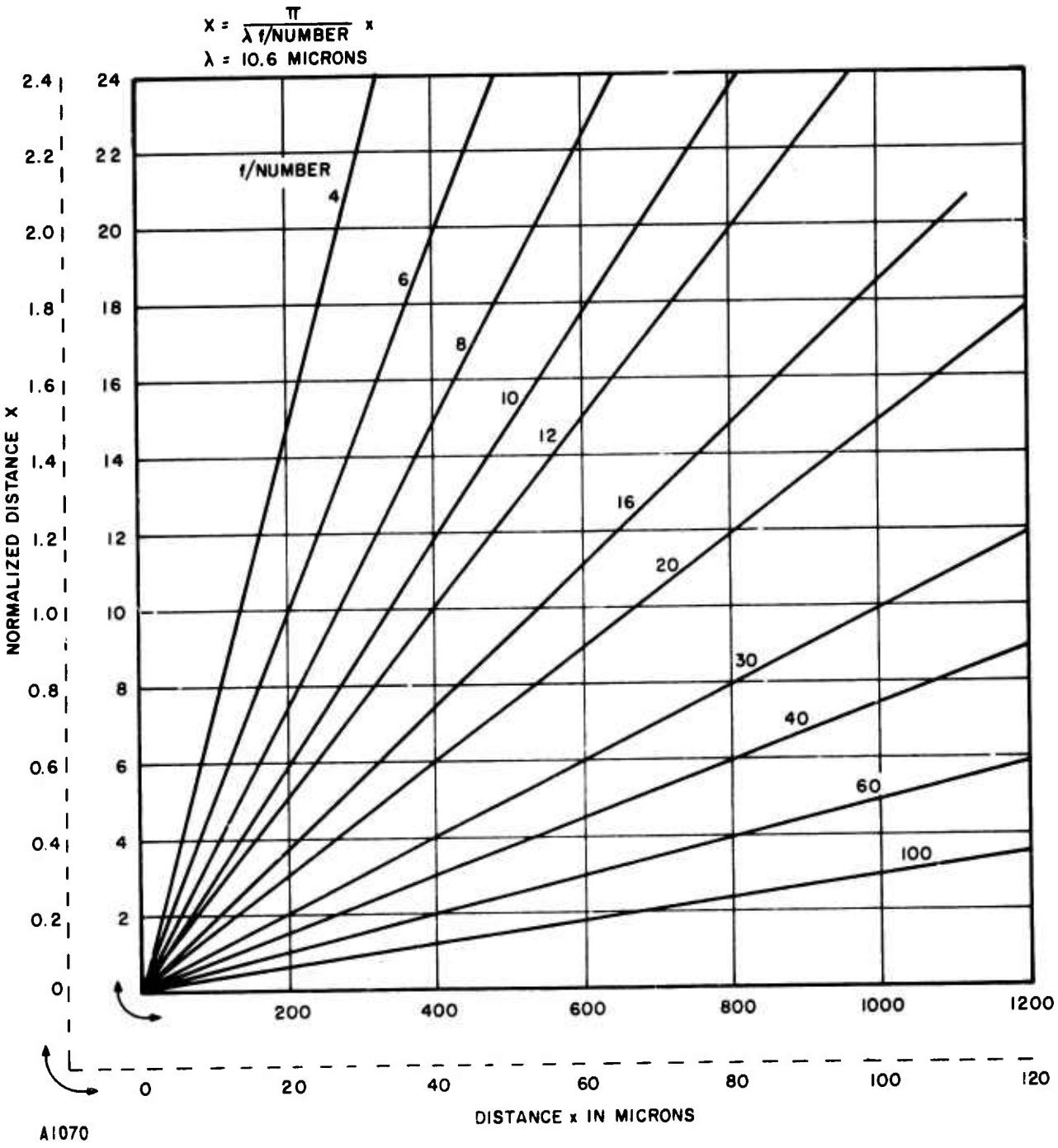

FIGURE 2-3. NORMALIZED MIXER DIMENSIONS

and substituting

$$A = \frac{k\rho}{f}\left[(x + x')^2 + (y + y')^2\right]^{1/2}$$

$$\psi = \arctan\frac{(x + x')}{(y + y')}$$

gives

$$I_o = \int_o^a \rho\left[\int_o^{2\pi} e^{iA\sin(\emptyset' + \psi)}\, d\emptyset'\right] d\rho$$

the inner integral (I_1) may be expanded into Bessel functions by means of the Jacobi-Anger formula (reference 7) into

$$I_1 = \int_o^{2\pi} J_o(A) + 2\sum_{k=1}^{\infty}\left\{J_{2k}(A)\cos\left[2k(\emptyset' + \psi)\right] + iJ_{2k-1}(A)\sin\left[(2k - 1)(\emptyset' + \psi)\right]\right\} d\emptyset'$$

Integrating gives 2π for the first term and zero for both the sine and the cosine terms; therefore,

$$I_o = 2\pi\int_o^a \rho\, J_o\left\{\frac{k\rho}{f}\left[(x + x')^2 + (y + y')^2\right]^{1/2}\right\} d\rho$$

Integrating, by means of Lommel's Integral (reference 7), gives

$$I_o = 2\pi a^2\,\frac{J_1\left\{\frac{ka}{f}\left[(x + x')^2 + (y + y')^2\right]^{1/2}\right\}}{\frac{ka}{f}\left[(x + x')^2 + (y + y')^2\right]^{1/2}}$$

This expression gives (within a multiplicative constant) the electric field distribution in the image plane (x, y), in terms of the direction of arrival (α', β') of a plane wave incident on the receiving aperture. Where (α', β') are referred to the image plane (x', y') by the previous equations. The expression describes a diffraction field of the form

$$\frac{J_1(X)}{X}$$

in two dimensions, with center displaced off-axis to a new origin ($-x'$, $-y'$).

Consider, now, the local oscillator beam which is incident on the image plane from a direction

$$\bar{n} = \bar{i}\,\epsilon + \bar{j}\,\delta + \bar{k}\,\mu$$

Again, defining a reference vector ($\bar{r}'$) in the image plane as $\bar{r}' = \bar{i}\,x + \bar{j}\,y$, and the phase difference over the image plane as

$$\Delta' = k\,\bar{r}' \cdot \bar{n}' = k(\epsilon x + \delta y)$$

Therefore, the field at the image plane, due to the local oscillator, may be represented by

$$\bar{E}_{LO}(x,y) = E_{LO}\, e^{-i\omega_o t}\, e^{ik(\epsilon x + \delta y)}$$

The fields of the received signal, and the local oscillator at the image plane (the mixer is placed here), are now combined by addition (again assuming that the polarizations of the two components are aligned) and the intensity of the resultant computed:

$$I_i = \left\langle \left(E_{LO} + E_p\right)^2 \right\rangle = \frac{1}{2T} \int_{-T}^{T} \left(E_{LO}^2 + E_p^2 + E_{LO} E_p^* + E_{LO}^* E_p\right) dt$$

The period of integration (2T) is taken very long compared to the period of the infrared frequency, but short compared to the period of the frequency difference introduced by the two cross terms. Therefore, the first two terms in the intergrand result in DC outputs from the mixer and are of no interest at this point. The two cross terms result in the

intermediate (IF) signal. The mixer responds to the real parts of these last two terms and it can be shown by direct substitution that

$$R_e\left(E_{LO}\,E_p^*\right) = R_e\left(E_{LO}^*\,E_p\right)$$

so that only one of these terms need be considered further. Moreover, the mixer responds to the integrated intensity, over its surface, so that the mixer output is given by

$$I_m = M \cdot 2\,R_e \int_{\substack{\text{mixer}\\ \text{area}}} \left(E_{LO}E_p^*\right)\,dA$$

$$= \frac{M\,2a^2k}{f}\,E_L E_T \int_{\substack{\text{mixer}\\ \text{area}}} \sin\left[\left(\omega_T - \omega_o\right)t + k\left(f + \epsilon x + \delta y\right)\right]\cdot$$

$$\frac{J_1\left\{\frac{ka}{f}\left[(x+x')^2 + (y+y')^2\right]^{1/2}\right\}}{\frac{ka}{f}\left[(x+x')^2 + (y+y')^2\right]^{1/2}}\,dA$$

where M is a proportionality constant relating the intensity at the mixer to the amplitudes of the IF signal output. Letting

$$C = \frac{M\,2a^2\,k\,E_L\,E_T}{f}$$

and assuming a square mixer element, gives

$$I_m = C \int_{y_1-\Delta y}^{y_1+\Delta y} \int_{x_1-\Delta x}^{x_1+\Delta x} \sin\left[\left(\omega_T - \omega_o\right)t + kf + k(\epsilon x + \delta y)\right]\cdot$$

$$\frac{J_1\left\{\frac{ka}{f}\left[(x+x')^2 + (y+y')^2\right]^{1/2}\right\}}{\frac{ka}{f}\left[(x+x')^2 + (y+y')^2\right]^{1/2}}\,dx\,dg$$

where

(x_1, y_1) = coordinates of the center of the square mixer

$(2\Delta x, 2\Delta y)$ = dimensions of the square mixer

In this equation, the argument of the sine term consists of three parts. The first part is the time-varying component that produces the IF signal; the second part represents a fixed phase that can be dropped without loss of generality, so long as $(\omega_T - \omega_o)$ is not equal to zero; the third term gives a variation in spatial phase across the mixer, caused by tilt in the local oscillator phase wavefront with respect to the mixer surface. When the local oscillator propagation direction and the mixer surface normal, coincide ($\epsilon = \delta = o$) and the third term disappears.

The Bessel function term gives an intensity pattern that is similar to the Airy disc field pattern rather than the square of the field pattern. This is brought about by the linearizing effect of a high-level local oscillator field and selection of the resulting IF component, only.

B. COMPUTED PATTERN

The integral (I_m) gives the IF signal output from a mixer element under a variety of conditions. By means of a digital computer, values of (I_m) were computed for several sets of parameter values.

When the coordinates of the center of the square mixer (x_1, y_1) are the variables, one obtains the mixer output at various positions in the image plane. This is the diffraction pattern seen by a mixer with finite dimensions. For various size mixers $(\Delta x, \Delta y)$, Figures 2-4 through 2-8 were obtained by sequencing x_1 (in increments of 50 microns) with y_1 set equal to zero. The other conditions were:

$\lambda = 10.6$ microns

f/number = 10

$2\Delta x = 2\Delta y$ = 10, 50, 80, 100, and 200 microns

With this selection of parameters, the diameter of the first dark ring is computed as 258 microns. This is seen in Figure 2-4. This pattern, for a 10- by 10-micron mixer, was intended as a probe of the image plane intensity distribution, as seen by an infinitesimal element. The results compared well with a plot of the function $J_1(x)/x$.

In Figures 2-5 through 2-8, the curves for 50, 80, 100, and 200 micron mixers have very similar patterns, although the absolute values of the mixer output vary strongly with mixer size. The dotted curve of Figure 2-8 is obtained by sequencing x_1 and y_1, simultaneously, in steps of 35 microns each. This gives the pattern along a main diagonal of the array. The main beam is only slightly affected by this diagonal sequencing and there is a slight inward shift of the sidelobes.

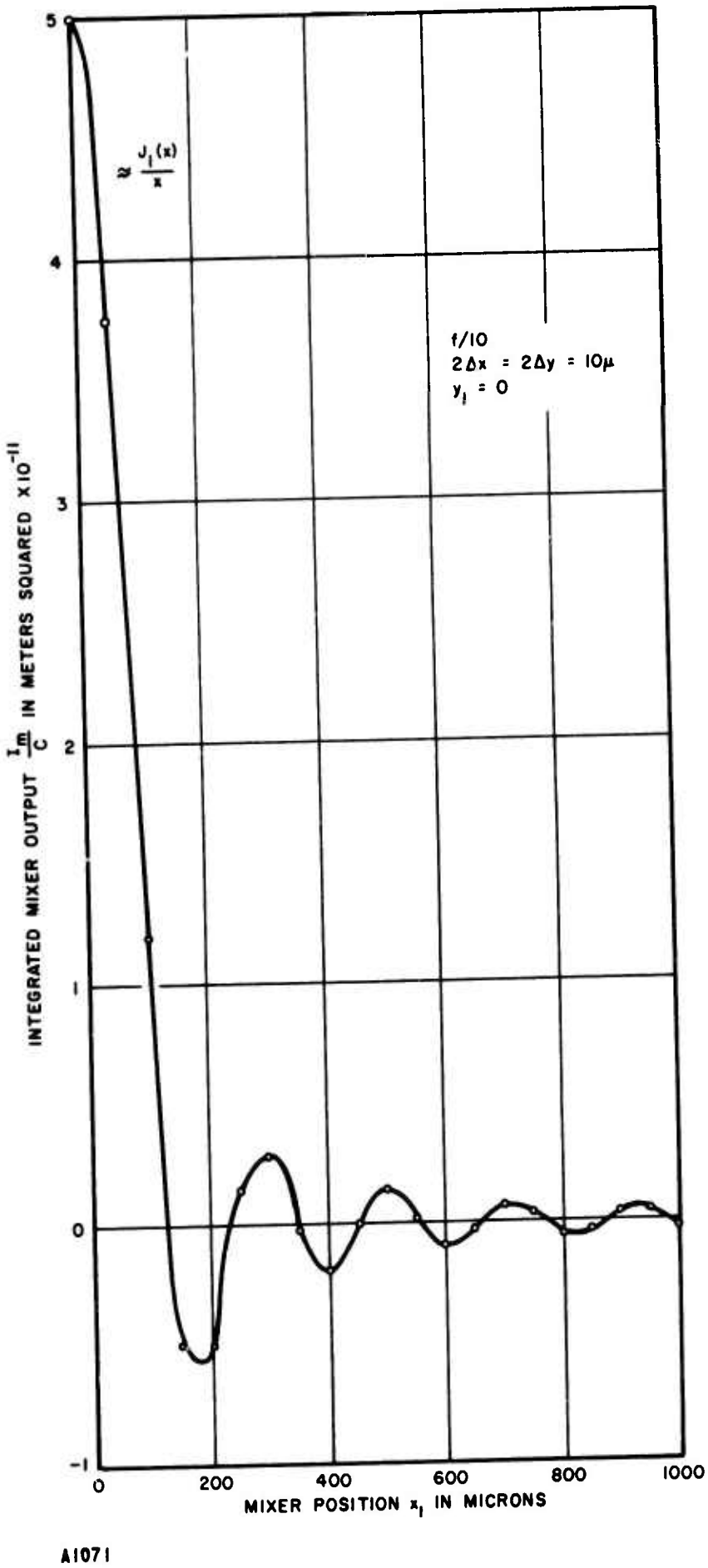

FIGURE 2-4. CALCULATED HETERODYNE RECEIVER BEAM PATTERN (10μ-SQUARE MIXER)

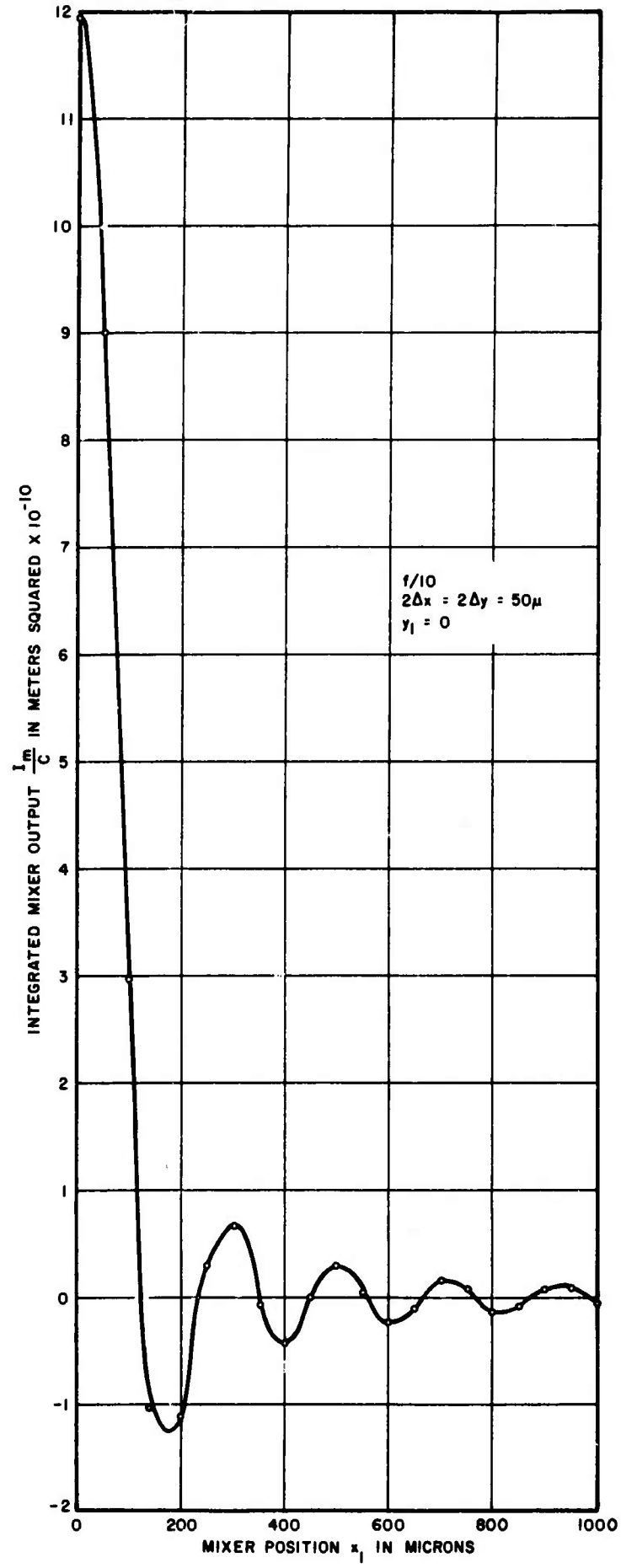

FIGURE 2-5. CALCULATED HETERODYNE RECEIVER BEAM PATTERN (50μ-SQUARE MIXER)

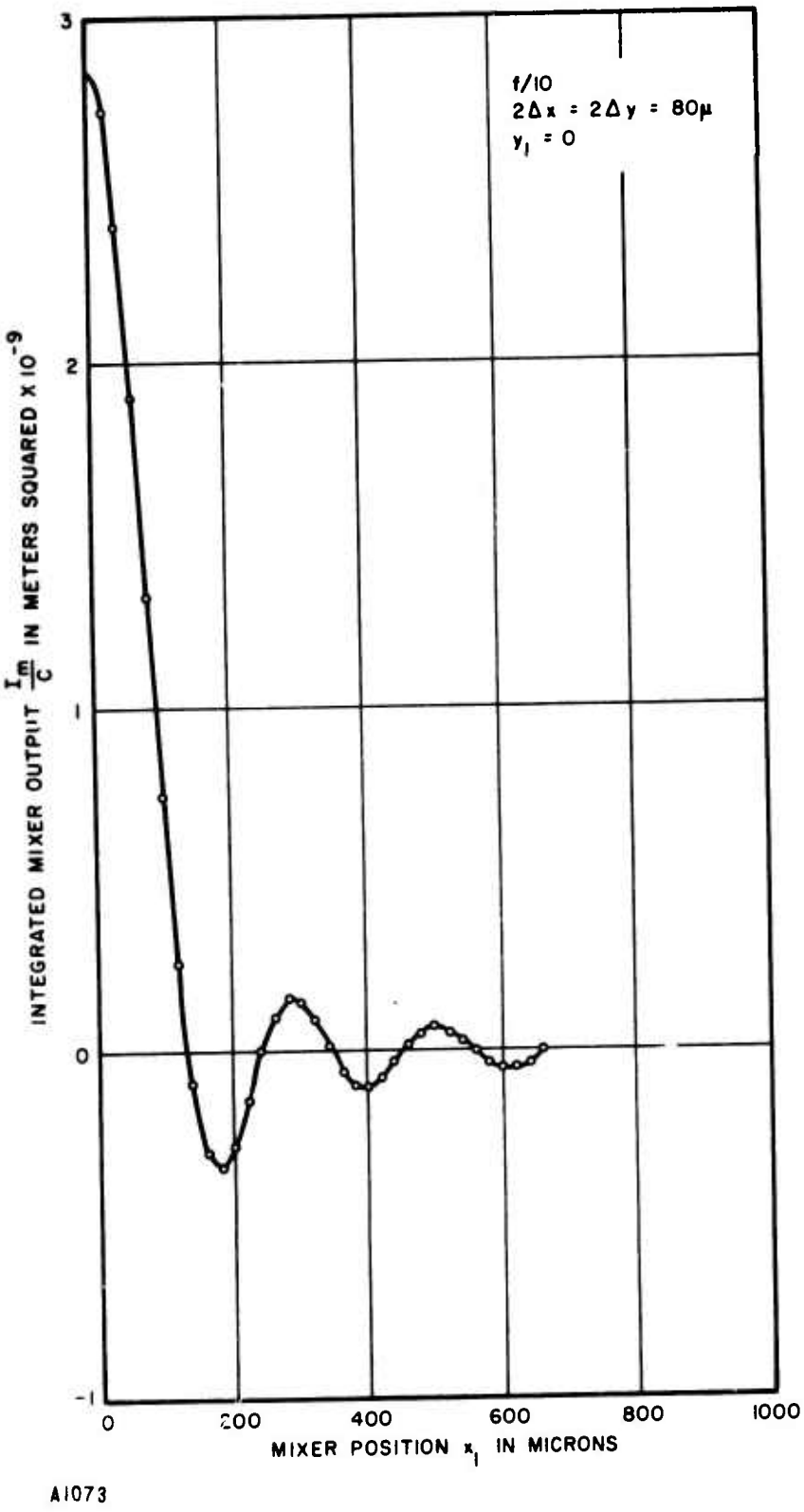

FIGURE 2-6. CALCULATED HETERODYNE RECEIVER BEAM PATTERN (80μ - SQUARE MIXER)

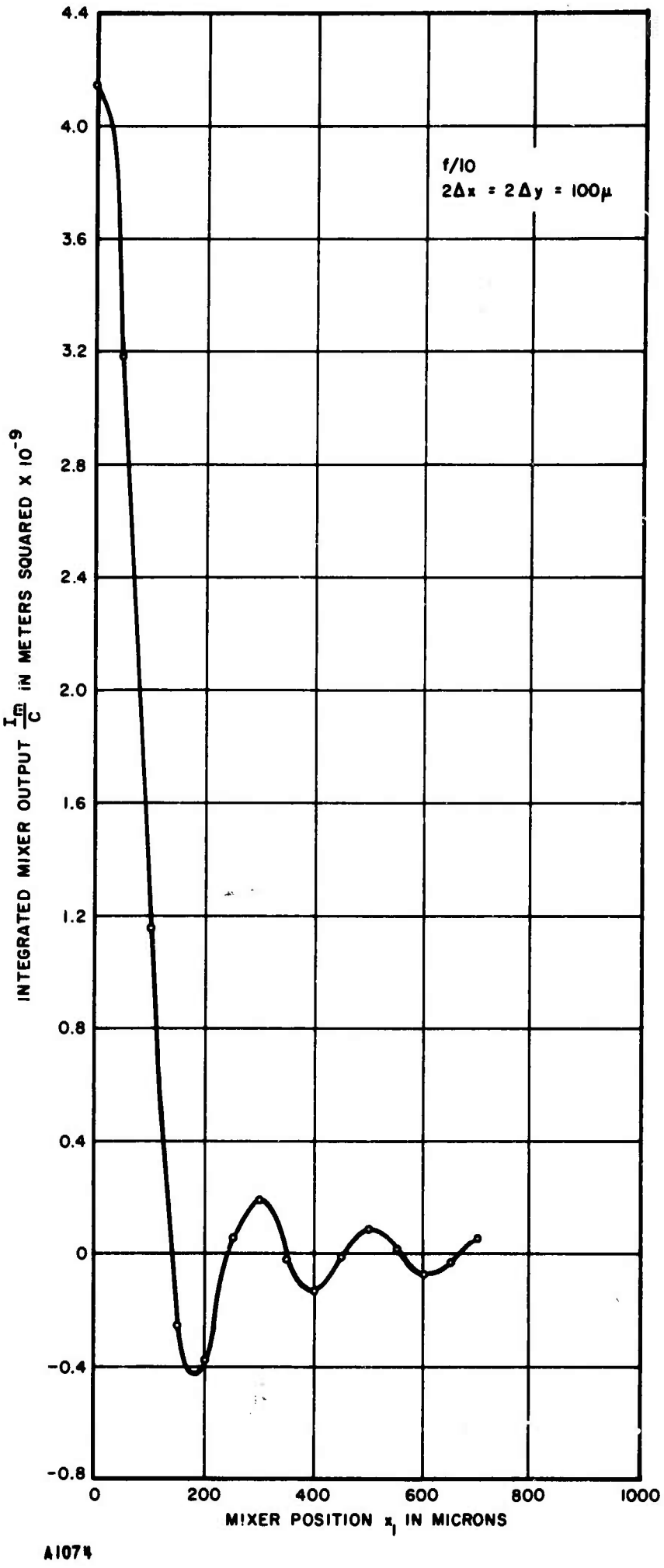

FIGURE 2-7. CALCULATED HETERODYNE RECEIVER BEAM PATTERN (100u - SQUARE MIXER)

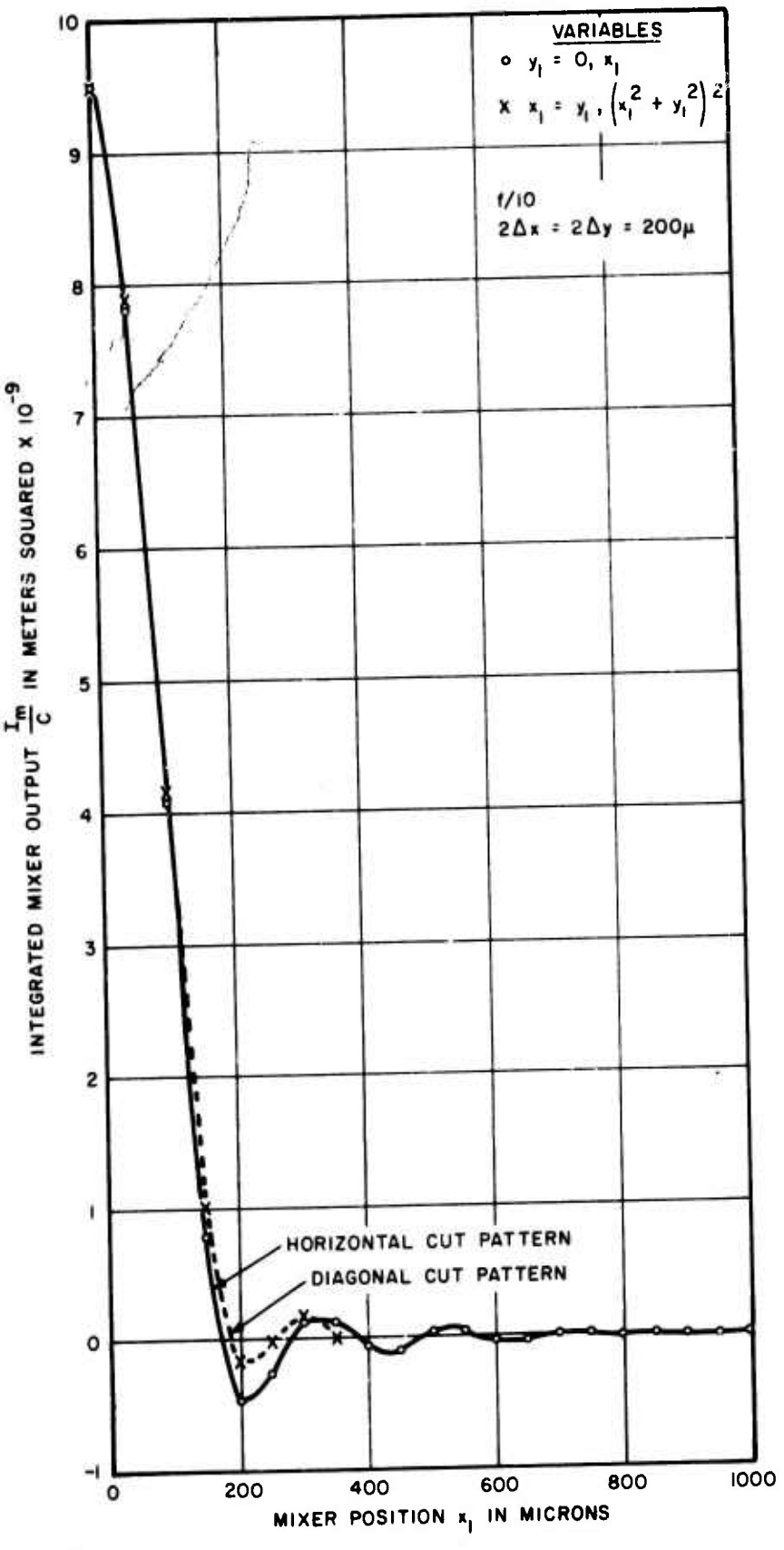

FIGURE 2-8. CALCULATED HETERODYNE RECEIVER BEAM PATTERN (200μ - SQUARE MIXER)

When the coordinates of the center of the signal patterns (x', y') are used as the variables in these integral computations, the curves obtained are identical with those obtained in Figures 2-4 through 2-8. Since sequencing (x', y') represents the process of scanning a point target across the field of view, the patterns obtained are the far-field diffraction patterns of the mixer element. The identity of the image plane intensity pattern and the far-field diffraction pattern is expected, and follows from the constraints of small-angle aberration-free imaging assumed in the derivation.

For each of the patterns of Figures 2-4 through 2-8, the response is down to 71 percent of the peak value (-3 db) when the spot center is 55 microns from the centers of two adjacent mixers.

For the 50, 80, and 100 micron mixer elements and an f/10 system, there is no overlapping of one mixer by the adjacent one, so that -3 db crossovers are, in principle, feasible.

With 200-micron mixer elements (at f/10) two elements cannot have their centers 55 microns from the spot center. Interpolating between the results for the 100- and 200-micron mixer elements, and normalizing with respect to f/number gives a maximum size for the mixer element of 3.26 units of normalized distance (Figure 2-3). This corresponds to 0.11 mm at f/10, 0.44 mm at f/40, and 1.10 mm at f/100. (Of course, overlapping fields of view could be achieved by means of a beamsplitter, but a loss in energy is incurred.)

Diffraction patterns were also computed for a skewed local oscillator wavefront $(\epsilon, \beta) \neq 0$. It was seen that when the local oscillator wavefront makes an angle of 5 milliradians, with respect to the mixer surface and the image plane, the pattern is negligibly affected out to 500 microns (at f/10) from the center. At 500 microns, a phase reversal occurs on either side of the spot center. This phase reversal, caused by local oscillator skewing, can have significant effects on coherent signal processing and is being investigated further.

The integral describing the IF signal output may be normalized by the following substitutions:

$$X = \frac{ka}{f} x = \frac{\pi}{\lambda F} x$$

$$Y = \frac{ka}{f} y = \frac{\pi}{\lambda F} y$$

where $F = \frac{f}{2a}$ = f/number of the optical system to give

$$I_m = C\left(\frac{\lambda F}{\pi}\right)^2 \int_{\frac{\pi}{\lambda F}(Y_1-\Delta Y)}^{\frac{\pi}{2F}(Y_1+\Delta Y)} \int_{\frac{\pi}{\lambda F}X_1-\Delta X}^{\frac{\pi}{2F}X_1+\Delta X} \sin\left[\left(\omega_1 - \omega_o\right)t + 2F(\epsilon X + \delta Y)\right] \cdot \frac{J_1\left\{\left[(X+X')^2 + (Y+Y')^2\right]^{1/2}\right\}}{\left[(X+X')^2 + (Y+Y')^2\right]^{1/2}} \, dX\,dY$$

In this form, it is apparent that the only characteristic of the optical system (within the limitations imposed by the assumptions used in the derivation) that affects the IF signal output is its f/number. The normalized coordinates (X, Y) represent the ratios of linear dimensions in the image plane to the spot diameter.

For ease of conversion, the transformation between actual and normalized dimensions has been plotted in Figure 2-3 (for a range of f/number and a wavelength of 10.6 microns). This permits one to apply the patterns computed for one set of parameters to other conditions.

C. PATTERN MEASUREMENTS

1. GENERAL

To verify the computed diffraction patterns and to provide a means for testing actual array responses, a coherent optical pattern measuring range, operative at 10.6 microns, was designed, assembled, and put into operation. The antenna range setup is shown in Figure 2-9, and its descriptive block diagram in Figure 2-10.

The CO_2 laser used here delivers several watts CW, and is mounted below the optical bench (Figure 2-11). This was done in order to provide more room for the antenna range, and to ensure operation in the far field of the laser.

The antenna range is basically a homodyne setup, in which the 10.6-micron laser output is split into a local oscillator beam and a signal beam which are individually shaped and then recombined and detected by a mixer element. The signal beam is mechanically chopped and expanded by means of a short focal-length lens, to provide a large diameter beam. This beam illuminates another lens that simulates the receiving aperture of the system. The latter lens is made small, with respect to the expanded beam diameter, to approximate the aperture illumination by a plane wave with uniform illumination across the aperture. The local oscillator beam and signal beam are combined colinearly with the signal beam focused onto the mixer in the image plane of the receiving aperture.

The mixer (in its dewar) is shown mounted on vertical and horizontal translation stages. In the horizontal plane, it is motor-driven and tied directly into a X-Y recorder.

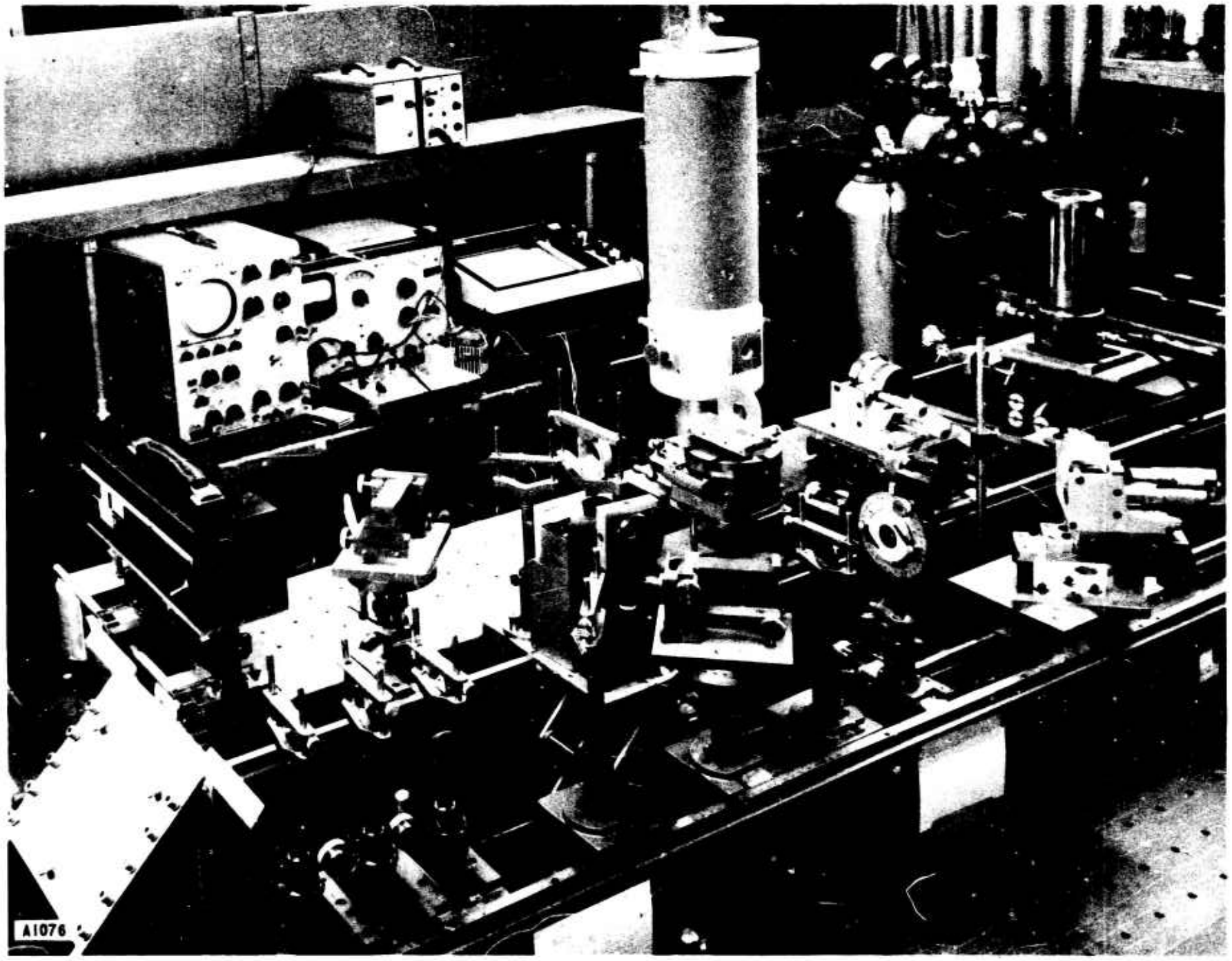

FIGURE 2-9. COHERENT OPTICAL ANTENNA PATTERN MEASURING RANGE OPERATING AT 10.6 MICRONS

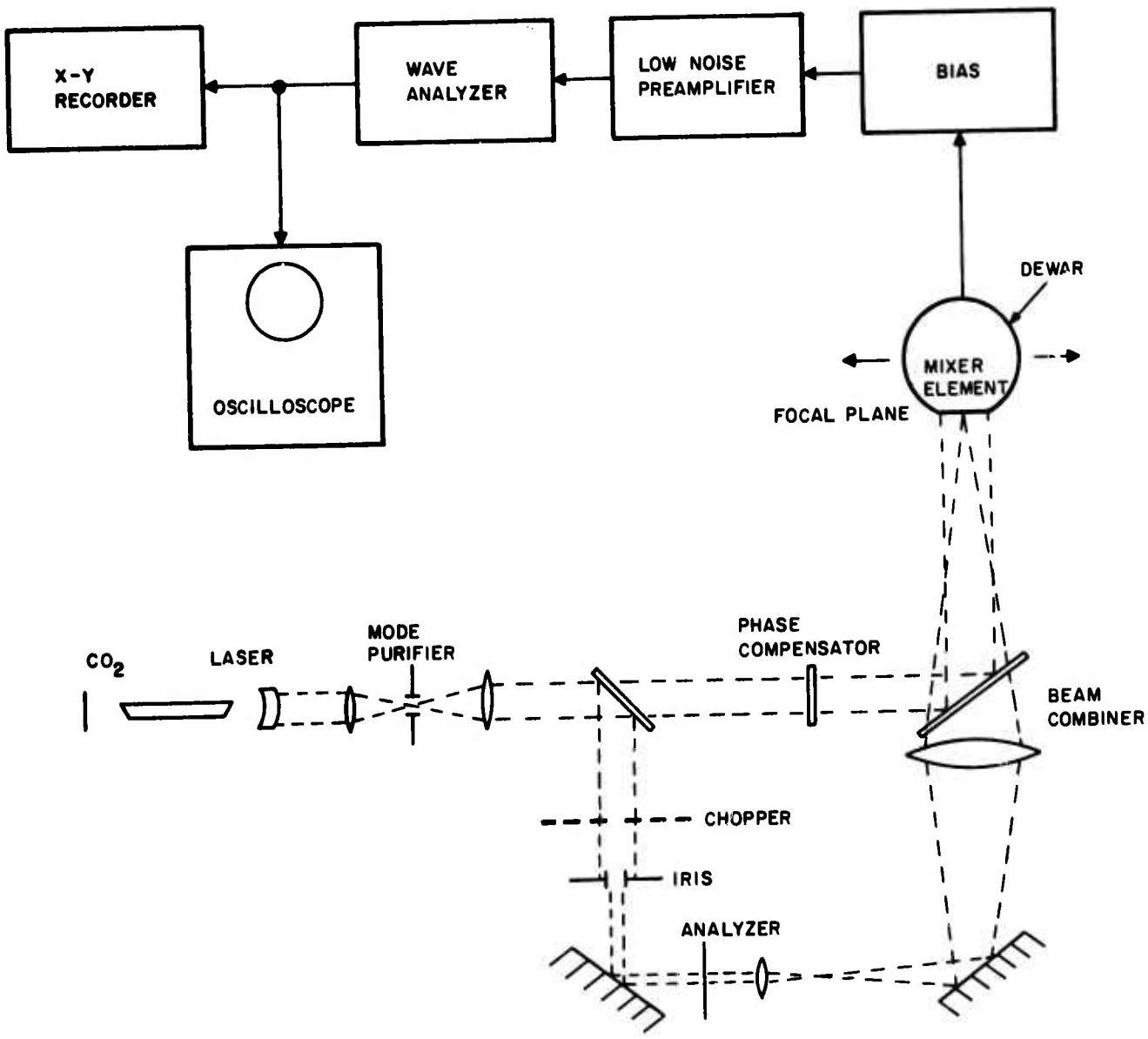

FIGURE 2-10. SCHEMATIC DIAGRAM OF COHERENT OPTICAL ANTENNA PATTERN MEASURING RANGE

Other items, shown in the photograph, include a mode purifier that spatially filters the beam, and a helium neon laser used in the optical alignment of the system.

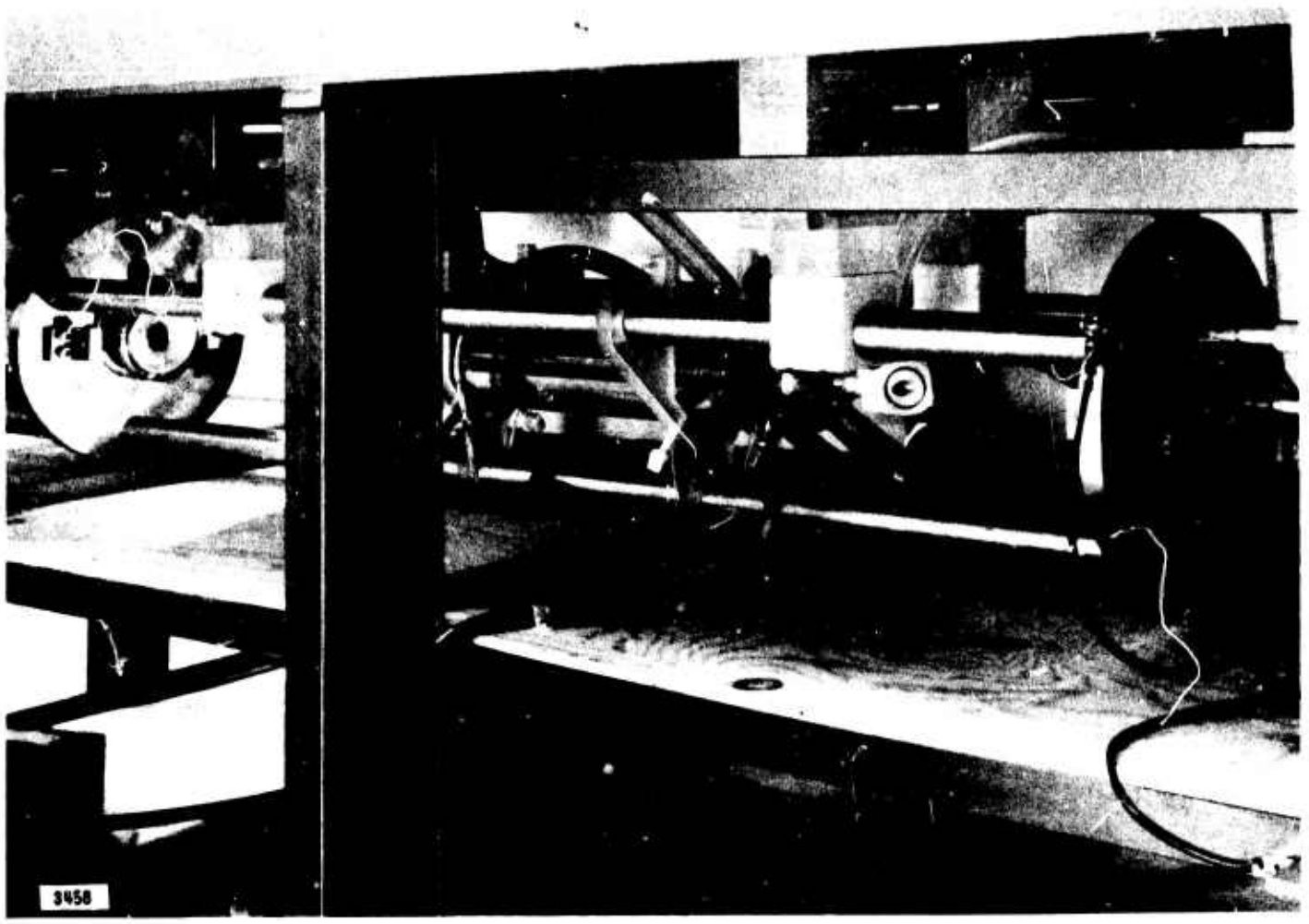

FIGURE 2-11. CO_2 LASER

2. TEST RESULTS

A number of diffraction patterns were measured. They are shown as plots of the mixed signal voltage as a function of mixer position in the image plane of the receiving lens. The parameters varied in these tests were the f/number of the receiving optics, the detector size, and the diameter of the expanded beam at the receiving aperture.

In one experiment, a 275-micron Ge:Au detector was used with a 100-micron aperture mounted very close to the front surface of the detector. The receiving optical system had an f/number of 10, with the lens illuminated by a large-diameter beam, thereby approaching the approximation of a uniform plane wave.

A vertical cut through the focused spot was taken and the measure data is shown in Figure 2-12. A calculated curve, for the same parameters is also shown in Figure 2-12

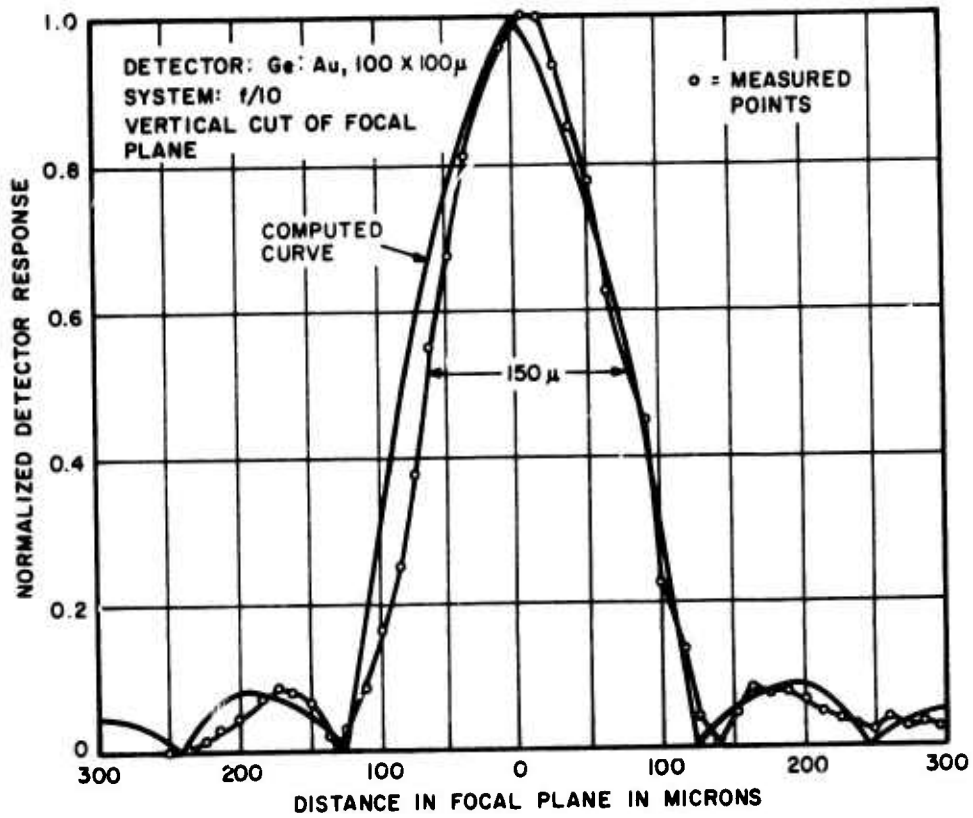

FIGURE 2-12. COMPARISON OF MEASURED AND CALCULATED INFRARED ANTENNA PATTERNS IN IMAGE PLANE

for comparison . The width of the beam at the points where the peak value falls to 50 percent is calculated as 160 microns and measured to be 150 microns (Figure 2-12) well within experimental error. The width of the first null in the pattern is calculated to be 280 microns (and measured as 270 microns). Similarly, the position of the peak of the second ring, and the intensity expected at that point, are also in very close agreement; the peaks occurring at 350 microns apart for the calculated curve and 350 microns apart for the experimental. Measurements beyond this value were limited by noise in the system. It can be concluded that the measured shape of the image plane pattern (which corresponds to the far-field diffraction pattern) is in very close agreement with the computer predictions.

With an f/8 system and the same mixer, horizontal cuts through the focal plane were made, automatically, and plotted on the X-Y recorder, rather than point-by-point. The results are given in Figures 2-13 and 2-14. Figure 2-13 shows the signal intensity alone with, and without, an Irtran I attenuator in the system. Figure 2-14 shows the local oscillator alone, and the mixed signal for the f/8 system.

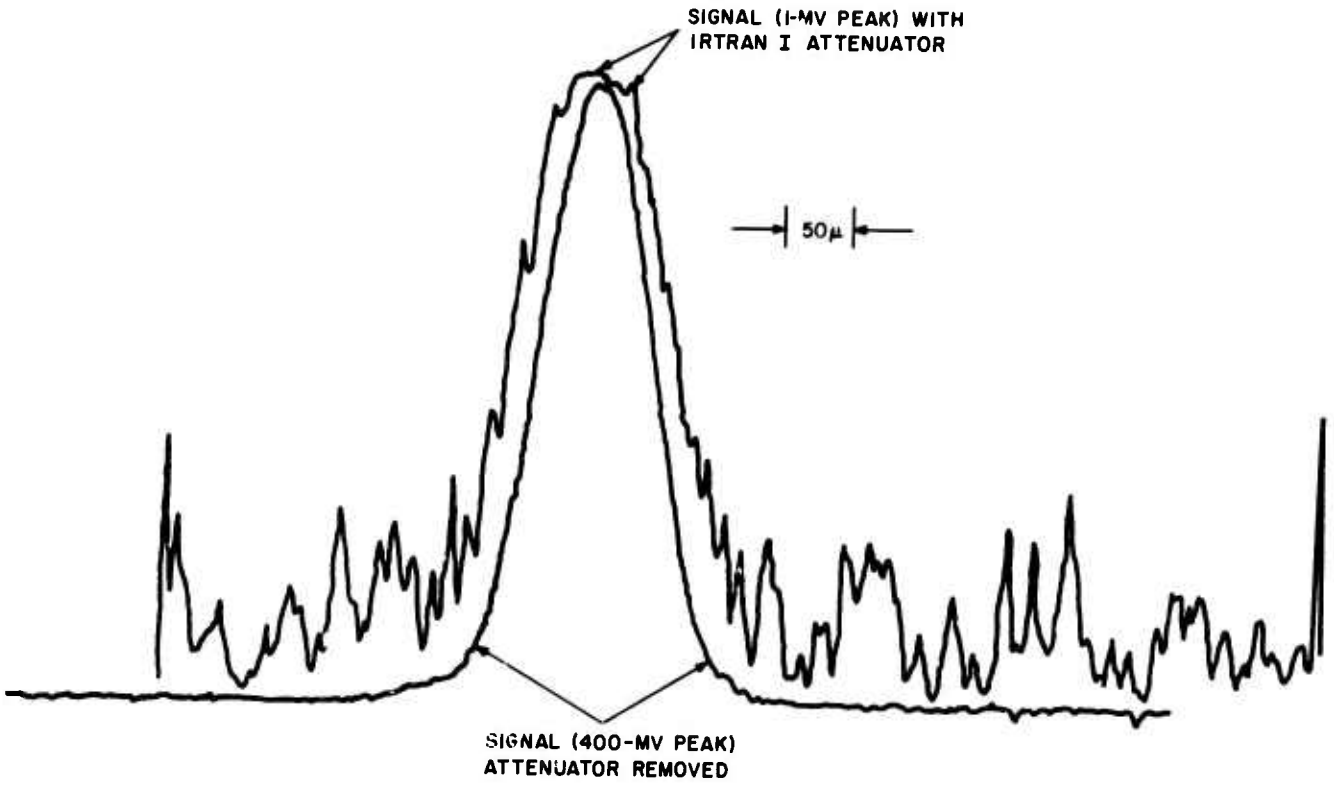

FIGURE 2-13. MEASURED SIGNAL INTENSITY FOR f/8 SYSTEM WITH AND WITHOUT OPTICAL ATTENUATOR

The measured mixing pattern is seen to be narrower than that which was calculated. As the f/number is reduced, a greater portion of the receiving lens is blocked by the beam-combining optics. It has been shown that as the obscuration of the center of the lens is increased, the mainlobe becomes narrower and the sidelobes increase in intensity (reference 8). Both of these phenomena can be seen in Figure 2-14, since the measured pattern is somewhat narrower than expected and the sidelobes are approximately double the predicted intensity. (The effects of obscuration were not included in the computed patterns.)

The third pattern (Figure 2-15) is for the same Ge:Au mixer, but with the 100-micron aperture removed, exposing the full 275 microns. The f/number of the system was increased to 12.25 and the illumination across the aperture was changed. A uniform intensity distribution across the aperture is no longer a good approximatation and an incomplete Gaussian distribution was considered (reference 9). This is a Gaussian distribution truncated by an aperture. The effect of this truncation is to broaden the far-field pattern. A taper ratio of 4, which represents cutting off the Gaussian curve at the point where the intensity is 25 percent of the peak, is a good approximation of the experimental setup.

The calculated curve, to which the data must be compared, is shown in Figure 2-16. The width of the pattern is 460 microns for a uniform illumination. For an

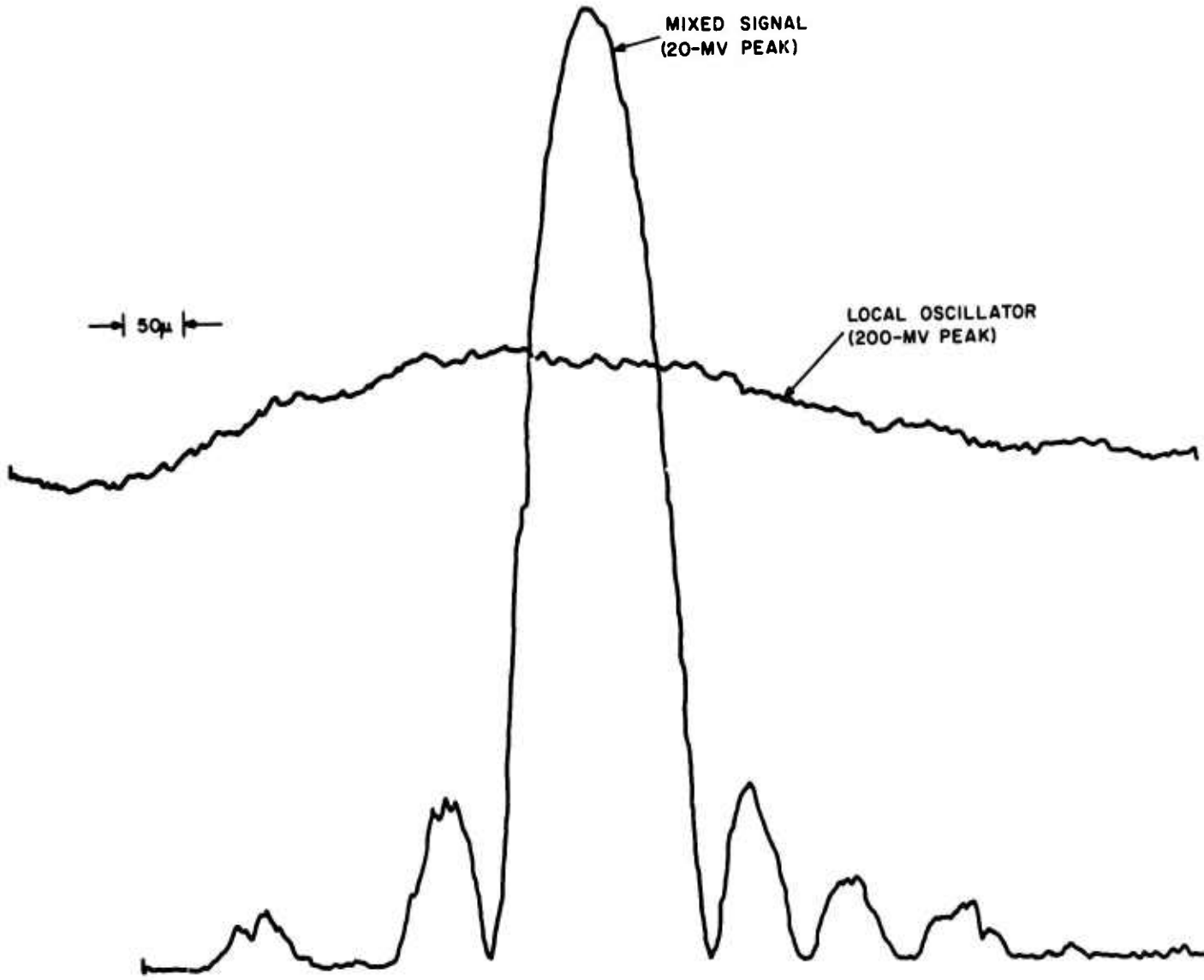

A1081

FIGURE 2-14. MEASURED MIXED SIGNAL AND LOCAL OSCILLATOR INTENSITIES FOR AN f/8 SYSTEM

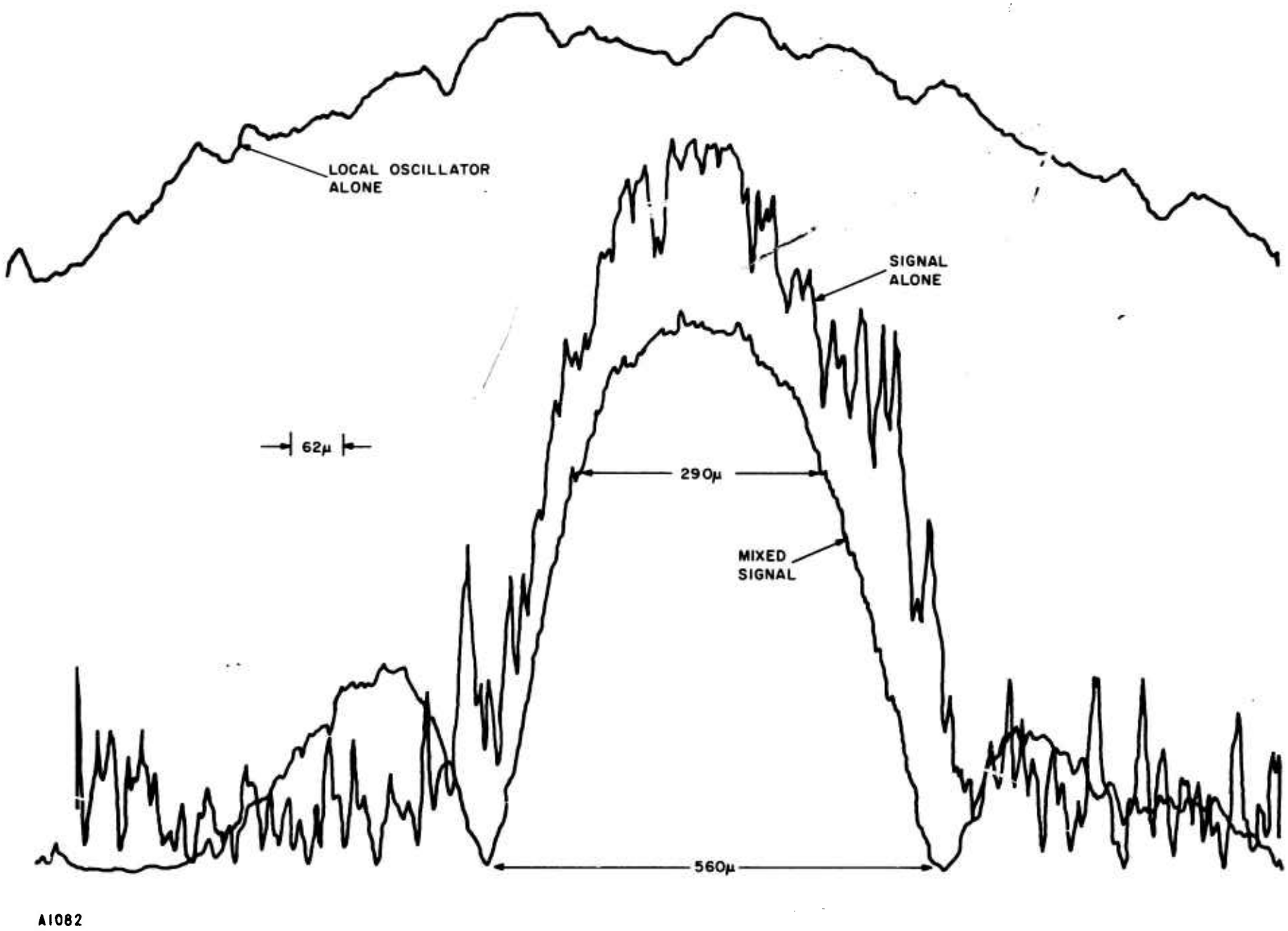

FIGURE 2-15. MEASURED MIXED SIGNAL, LOCAL OSCILLATOR, AND SIGNAL INTENSITIES FOR A 275-MICRON Ge:Au MIXER

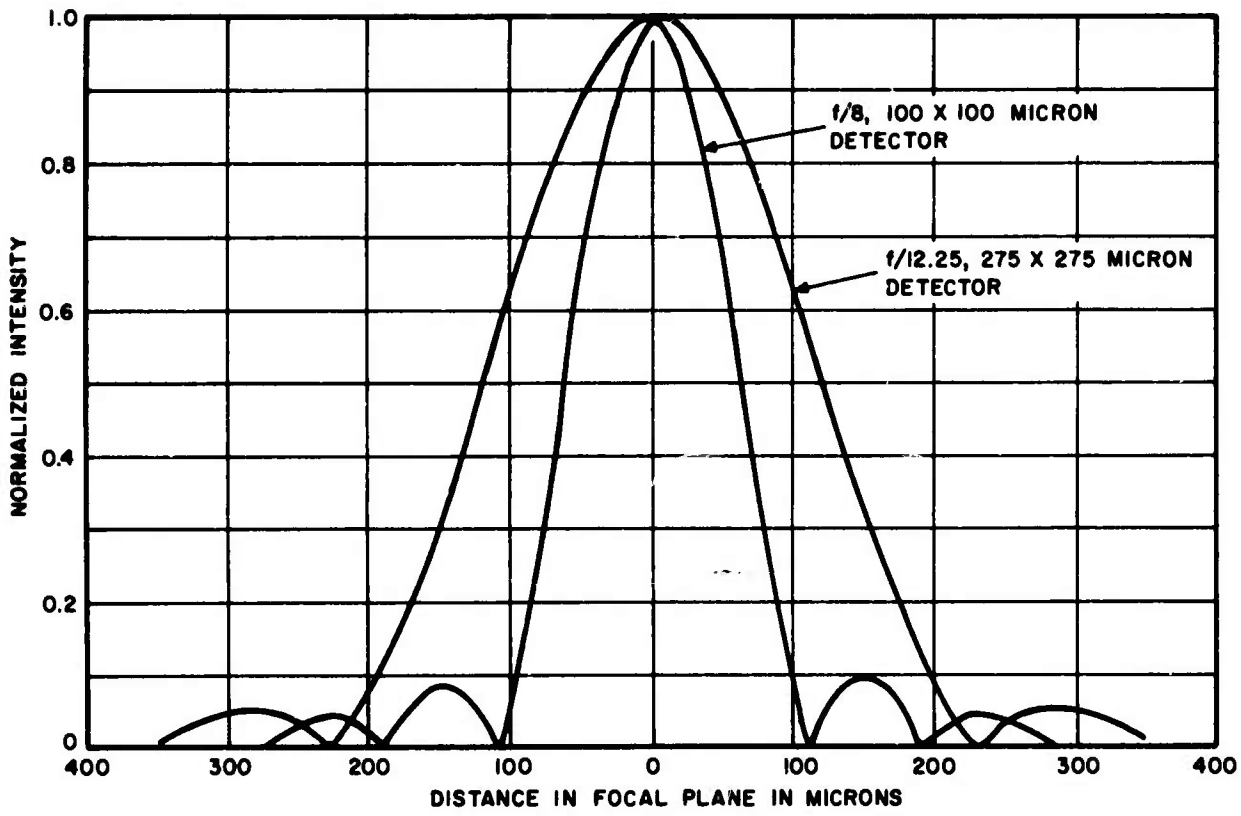

FIGURE 2-16. COMPUTED INTENSITY DISTRIBUTION IN FOCAL PLANE

incomplete Gaussian of taper ratio 4, the pattern should be 1.26 times as large as that expected for a uniform illumination or 580 microns. This compares well with the measured width of 560 microns.

The sidelobes (Figure 2-15) are higher than were expected for the parameters used. This is believed due to slight saturation in the mixer, caused by a nonoptimum choice of bias circuit parameters during this run.

D. DISSECTION OF IMAGE PLANE

1. GENERAL

The design of a two-dimensional array requires as one principal task the partioning, or dissection, of the image plane of the receiving aperture into well defined and carefully selected areas whose photon flux is collected by associated mixer elements. This section describes techniques for dissecting the image plane and guiding the infrared energy to the individual mixer elements.

2. BEAM CROSSOVER

To permit continuous tracking of one, or several, targets across the field-of-view of the array when the system is operating near its sensitivity threshold, it is necessary that the individual beam patterns cross over their adjacent patterns at response levels not too far below their peaks. Experience in microwave system design indicates that a beam crossover approximately 3 db below peak represents a practical compromise between total angular coverage of the array, single-element photon capture efficiency, and permissible signal variations. Until definitive system requirements are available, crossovers in the region of -3 db will be used as the basis of the infrared coherent array design. Should another level of beam crossover appear desirable, after the detailed dimensions of the array elements have been fixed, the adjustment could be made by changing the f/number specification for the input optics.

Although much of the foregoing analysis may be normalized and expressed in terms of λ and f/number, the actual physical dimensions of the devices (rather than their normalized values) are of prime interest, because these directly affect the fabrication feasibility of the array.

Table I gives calculations of two critical dimensions; they are the spot diameter and the depth of focus (as a function of f/number at 10.6 microns). The spot diamenter is taken as the diameter of the first dark ring of the Airy disk, and the depth of focus is defined as the distance between the first on-axis nulls on either side of the geometrical focus.

TABLE I. CALCULATED VALUES FOR SPOT DIAMETER AND DEPTH OF FOCUS (AT 10.6 MICRONS)

f/Number	Spot Diameter $= 2.44\lambda f$ (mm)	Depth of Focus $= 4\lambda f^2$ (mm)
1	0.0258	0.042
4	0.1032	0.671
10	0.2580	4.240
20	0.5160	16.800
40	1.0320	67.100
100	2.5800	424.000

When no intervening optics are used, it is required that the image dissector and mixer elements be within a distance of each other corresponding to the depth-of-focus. At the image plane, the local oscillator wavefront, and that of the received signal, are approximately parallel to each other, which condition is necessary for efficient mixing, and remain so within the depth-of-focus.

Figure 2-17 shows the mixer output constant-voltage contours for a diffraction-limited spot. The plot is interpreted as follows. With the spot centered as shown, a mixer element centered on one of the constant db contours (and having dimensions less than or equal to the 3-db contour diameter) will have, as its response, the indicated db value below the peak response obtained at the spot center. The solid squares outline the areas assigned to each of the nine mixer elements when 3-db crossovers are required between adjacent elements, and likewise the dashed squares for 6-db crossovers. Dimensional calibrations are given for the normalized variable and an f/20 system.

For the 3-db crossover case, a spot centered at the point common to four mixer elements gives a response, in each of these elements, which is 6 db below the peak. For the 6-db crossover case, the response is down 18 db below peak. Since the latter situation could cause signal dropouts near threshold conditions, the 6-db crossovers are undesirable although the increased area available for each mixer element alleviates some array fabrication problems.

3. ARRAY ELEMENT EFFICIENCY

The array design must be such that the input signal energy is efficiently used in the mixing process. Unused signal energy degrades overall sensitivity of the system. Because of the requirements for cooling, cabling, electrical shielding, minimum mixer crosstalk, and array fabrication, it becomes necessary to provide space between mixer elements.

A filling factor σ is defined as the ratio of the area occupied by a mixer element to the total area assigned this element by the image phase dissection. For some of the image dissection methods described, values of σ as high as 90 percent can be expected. However, if no optical elements are used for image dissection, values of σ appear limited to 25 percent.

4. TECHNIQUES FOR IMAGE DISSECTION

Two basic approaches have been devised for efficient image dissection. In the first approach, the partitioned areas in the image plane are separated from one another to permit using relatively isolated mixer elements. This approach is most easily implemented for a moderate number of elements, such as nine in a 3×3 array. The partitioned areas of the image plane diverge from one another so that the mixer elements are relatively isolated and the array fabrication does not involve the development of new technology (beyond fabrication of individual mixer elements). The mixer elements may be fabricated, mounted, cabled, and tested separately, then arranged on a relatively large area mounting plate to accept the dissected image. Variations of this first approach using mirrors, wedges, and masked beamsplitters are discussed.

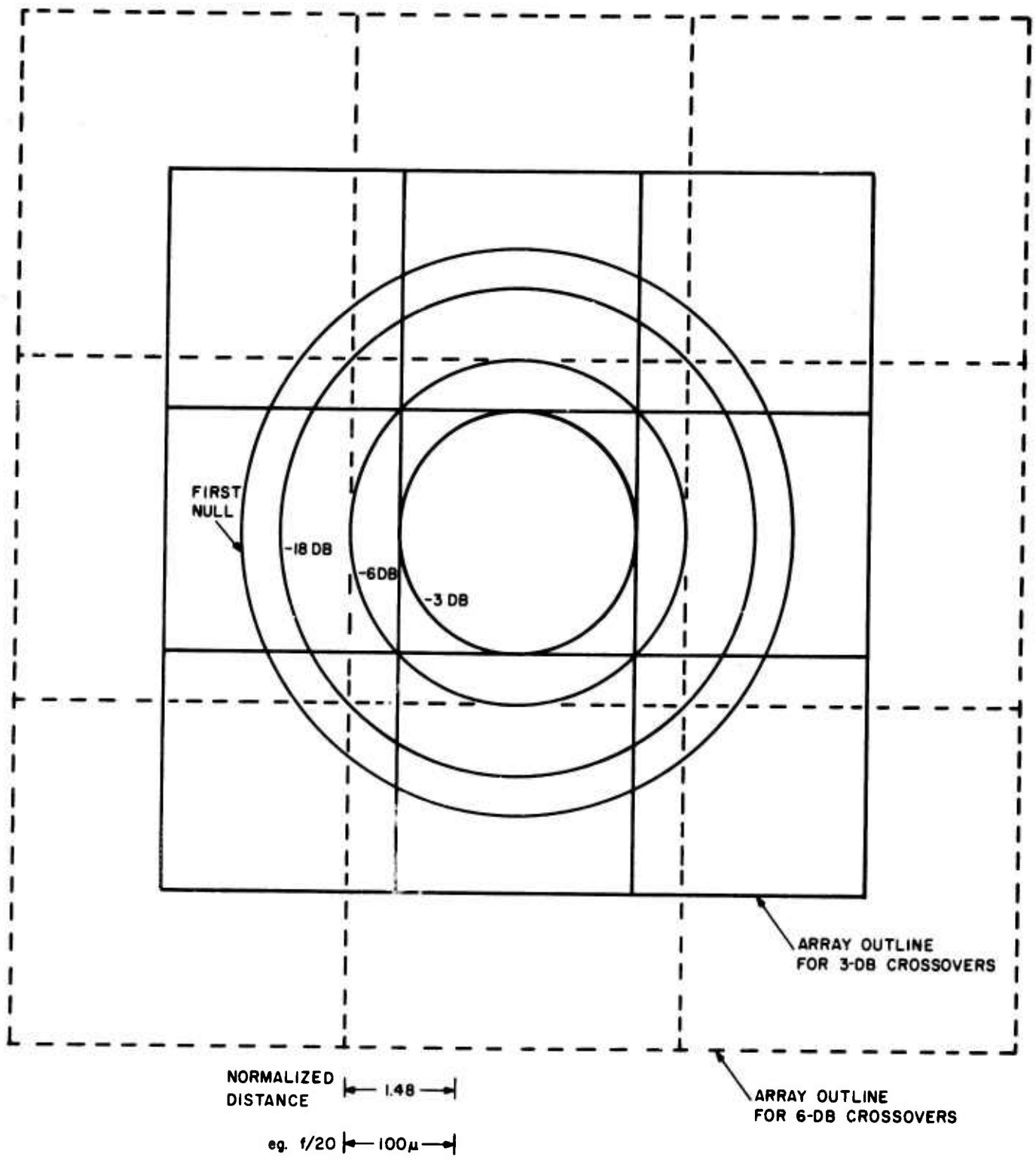

FIGURE 2-17. CONSTANT-VOLTAGE CONTOURS FOR DIFFRACTION-LIMITED BEAM IN FOCAL PLANE OF 3 x 3 ARRAY FOR 3- AND 6-DB CROSSOVERS

The second approach uses a high f/ number to increase the image size. Then, the partitioned areas are optically reduced to accommodate relatively samll detectors. There is no increase in the center-to-center spacing, which is set by the f/ number. However, there can be a very substantial increase in the geometrical filling factor. This approach can compactly accommodate large arrays (such as 100 elements in a 10 × 10 array).

For this second type of image dissection, where the partitioned areas do not diverge, significant array problems need to be solved. For example, with an f/40 spot the center-to-center spacing of the mixer elements is about 0.018 inch. This spacing must be maintained in two dimensions while accommodating the required cooling surface, cabling, and electrical shielding. Also, since the mixer element will most likely be made of germanium, or similar material, that requires a long element geometry (the mixer length is several times its width) to permit efficient photon absorption, the array problem is three-dimensional. One implementation of this approach, using microlenses, is discussed.

Preliminary computations on heat conduction, electrical shielding, stray capacitance, and cabling losses show that these aspects of the array present no prohibitive difficulties. The substrate requirements can be met by precision machine shop practices. The fabrication and mounting procedures for the mixer elements are similar to those used for single-element mixers, and new technology is not required. Many details remain to be resolved but the approach appears feasible. An important feature of this approach is its adaptability to larger arrays.

E. MULTIFACETED MIRRORS

A multifaceted mirror placed at the image plane can be used to dissect the signal spot. Arrangements for 2 × 2, and 3 × 3 image dissectors, are shown in Figure 2-18. The mixers are placed within the depth-of-focus length of the mirrors, or transfer lenses are used to refocus at a greater distance.

Examination of Figure 2-18a shows that the central element in the larger array is accommodated by removing the reflecting material or piercing the substrate.

The reflections can be made almost lossless (approximately 99 percent). The filling factor is set by the quality of the edges between mirror facets, and it is estimated that 90 percent efficiencies can be achieved.

In considering an image dissection technique for future development, consideration should be given to its use with arrays larger than 3 × 3. The multifaceted approach does not appear compatible with very large arrays.

F. MULTIWEDGES

A beam of electromagnetic energy traversing a wedge of high-refractive-index material will be dissected by the discontinuities at the wedge edges and its segments dispersed into a divergent pattern. The mixer elements are then placed where the segments are sufficiently separated, but within the depth-of-focus length. As with the multifaceted

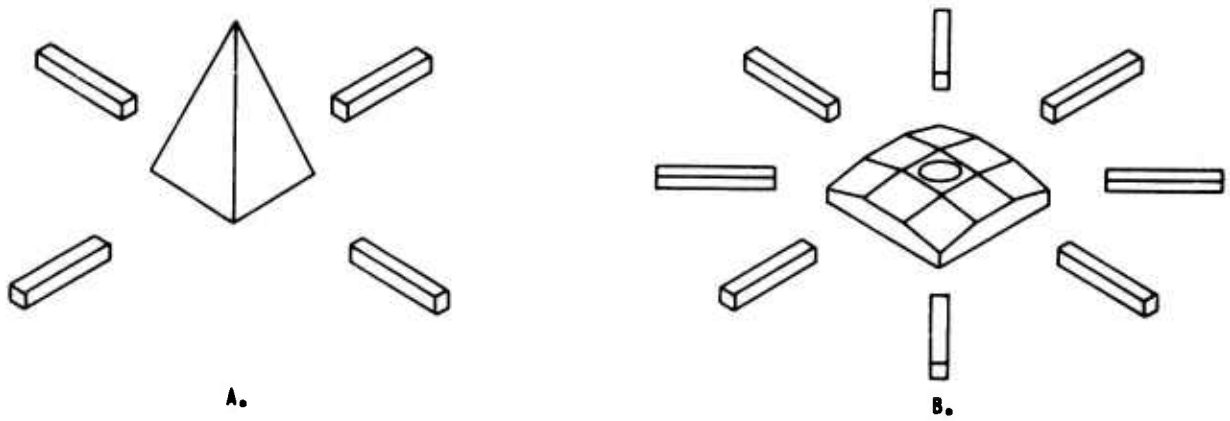

MULTIFACED MIRRORS

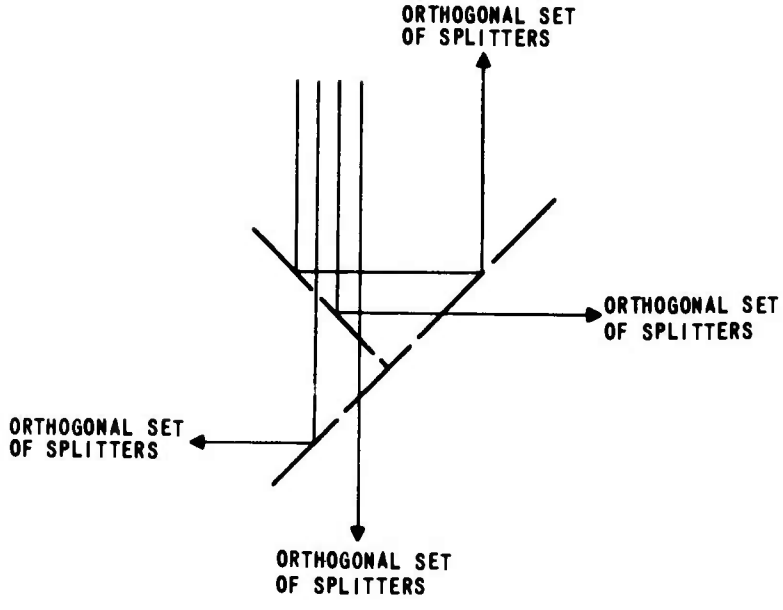

MASKED SPLITTERS

ARRAY OF MICROLENSES

FIGURE 2-18. IMAGE DISSECTORS

mirrors, if greater separation is required, or a better dimensional match is desired between the segments and mixer elements, an array of transfer lenses may be added.

Comparing this approach with the multifaceted mirrors, the wedges are somewhat lossier (estimated at 94 percent transmission, as compared to 99 percent with the mirrors) but the central element presents no special problem.

G. MASKED SPLITTERS

Image dissection can also be accomplished by using beamsplitters with alternate transmitters and reflecting strips on their surfaces. Figure 2-18c shows how this technique dissects the pattern in one dimension. Each of the four emerging strip beams must then be dissected along its length by repetition of the same technique at right angles to the first one. This approach lends itself most readily to a binary geometry. For a 4 × 4 array, a total of five sets of beamsplitters (shown in Figure 2-18) will provide signal for 16 separated mixer elements.

There is an obvious limitation to this approach, that is, the total path length from the first beamsplitter to the mixer element must not exceed the depth-of-focus length of the system. The feasibility of this approach is questionable, due to its fabrication intricacies. Hence this approach is not considered further.

H. MICROLENSES

This method is an example of the second basic approach to image dissection, wherein the emerging beams do not diverge with respect to one another, and the array elements are closely spaced. The image pattern of Figure 2-18d is dissected by an array of square lenses. At the focus of each lens is placed a mixer element that accepts the condensed energy from its associated segment. With an f/100 spot, a reduction of 5 to 1 provides a good match to the mixer element, a high filling factor, and sufficient room for cooling, cabling, shielding, and array fabrication. The resulting array of mixer elements is relatively compact, and the approach is extendable to much larger arrays than the 3 × 3 considered here.

Square germanium lenses (about 1 mm on a side) are within the state-of-the-art and can be assembled into arrays for efficient image dissection. It is estimated that a filling factor of 90 percent can be approached. These germanium lenses would be anti-reflection coated to give transmission factors near 94 percent.

I. FIBER OPTICS

Fiber optics may offer a suitable technique for incoherent low-resolution image dissection. However, the special requirements, here, for high resolution, phase sensitivity, and polarization-sensitivity mixing, raise serious questions concerning their suitability on this program. Excitation of a fiber by a plane wave usually, and often unpredictably, results in complex combinations of many dielectric waveguide modes with several polarization states existing at the output end (reference 10). The mode pattern at the output is also dependent

on the length of the fiber. In addition, there is strong evanescent-wave coupling between fibers that is enhanced for longer wavelengths and makes the beam crossover points difficult to design, while seriously increasing the optical crosstalk between elements.

The materials available for 10.6-micron fiber optics are relatively lossy; for arsenic trisulfide glass, an attentuation of 10 db, for a one-half inch fiber, has been reported (reference 11).

BLANK PAGE

III. 1.5-GHz MIXER DEVELOPMENT

A. APPROACH

The design of the 10.6-micron mixer for this program is governed by the following objectives:

- High sensitivity, with operation near the quantum-noise limit.
- Large instantaneous frequency response (10 MHz to 1.5 GHz).
- Low-noise, wideband IF amplifier optimally coupled with the mixer.
- Minimum power dissipation required for local oscillator and DC bias (to achieve required performance).
- Highest possible operating temperature.

In this section, experimental data toward the above objectives (on photoconductive mixers and analyses on photovoltaic 10.6-micron mixing) are presented.

B. PHOTOCONDUCTIVE MIXERS

A program recently completed at AIL (under NASA sponsorship) obtained explicit engineering equations useful in the design of optimum infrared receivers. These engineering equations involved such parameters as: local oscillator power, DC bias power, IF amplifier noise temperature, mixer-IF interface, mixer resistance, and mixer material parameters. The results of this analysis, with specific application to gigahertz bandwidth 10.6-micron high-sensitivity receiver development, have been published (reference 1).

In the approach that was developed, infrared mixer performance was expressed in terms of two principal factors:

- Noise attributable to the mixer element itself.
- IF amplifier noise referred to the mixer input through the conversion gain term, which quantitatively describes the ability of the frequency-translation process to convert the available infrared signal to IF signal.

Examination of the expressions for conversion gain and noise equivalent power provide the following criteria for quantum-noise-limited large-IF-bandwidth infrared mixer design:

- High mixer quantum efficiency
- Carrier lifetimes in the subnanosecond region
- Low mixer resistance, achieved by sufficient laser local oscillator power
- Short carrier transit times in the mixer
- Low mixer capacitance
- Linear mixer operation, including absence of carrier depletion due to excessive local oscillator power
- Low-noise IF amplifier

Only a few infrared detector materials are candidates for meeting the above criteria. These materials include Ge:Cu, Ge:Hg, Si:Al, HgCdTe and PbSn (Te, Se). Photoconductive Ge:Cu, in which compensation significantly decreases carrier lifetime, is a prime candidate. This material is useful for heterodyne operation from approximately 5 to 30 microns.

Measurements on compensated Ge:Cu, as a mixer material, were given in reference 1 and its successful application in a packaged unit is described in reference 2.

C. SELECTION OF PHOTOCONDUCTIVE MIXER MATERIAL

The development of a 1.5-GHz mixer-preamplifier combination for the present program is based on: (1) extending the technology initially developed under NASA contract for a single-channel 10.6-micron 1-GHz heterodyne receiver, and (2) examining other mixer materials.

While there are a number of interrelated parameters, the frequency response of a PC mixer element is largely limited by the carrier lifetime, τ. Figure 3-1 shows the variation of conversion gain (G) with IF frequency for three values of τ. Two ordinates are shown, depending on what value is taken for transit time. Note that a variation in G with IF frequency does not necessarily indicate that receiver sensitivity will vary in the same manner; what matters for quantum noise limited performance is the frequency range over which the conversion gain is sufficient to override IF amplifier noise. A gain-equalizing network may be used in the IF where receiver sensitivity has already been established.

Whereas frequency response increases with decreasing carrier lifetime, the available mixer gain increases with τ, resulting in a gain-bandwidth constraint. Figure 3-1 shows that in order to extend frequency response to 1.5 GHz, and beyond, it is desirable to reduce τ in order to increase G at the higher frequencies. This has the effect of decreasing G at the lower frequencies, but this is not necessarily a disadvantage since the IF noise factor is usually lower at the lower frequencies. The decrease in τ is accomplished by increasing the impurity-doping in the mixer element.

Since many of the design considerations are interrelated, the final choice of mixer material for the array will be determined by experimentation based on the underlying analytical considerations mentioned above.

The following sections present test data on nine mixers (five Ge:Cu, one Ge:Hg, one Si:Al, and two HgCdTe). The measurements were carried out using a low-noise broadband IF amplifier whose characteristics are described further in Section III-G. Work to increase the upper frequency limit of the amplifier is in progress.

D. COPPER-DOPED GERMANIUM

Copper-doped germanium photoconductive detectors offer the most promise for this application. Overall receiver sensitivity can be optimized by minimizing the ratio of the

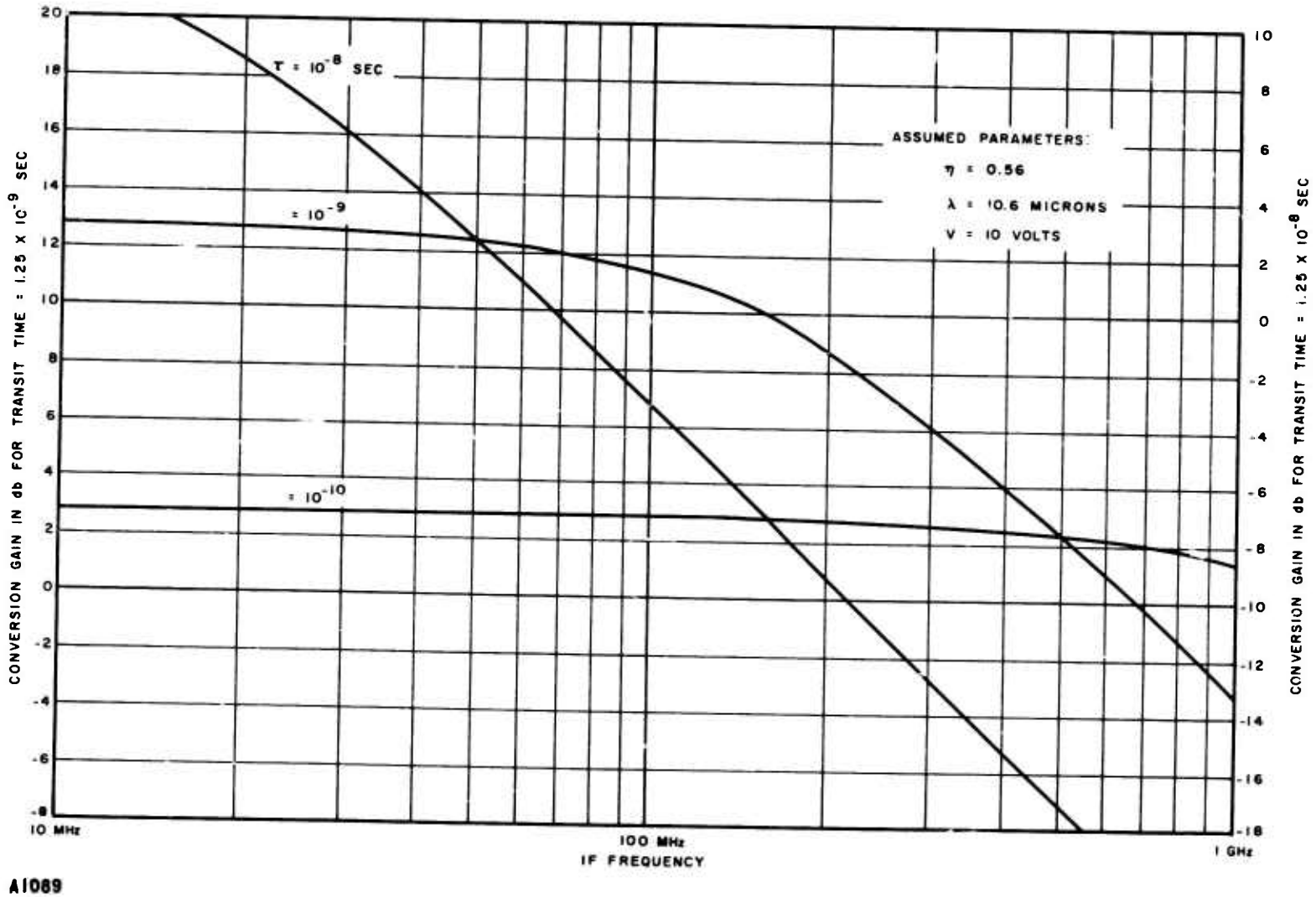

FIGURE 3-1. CALCULATED VARIATION OF CONVERSION GAIN WITH FREQUENCY FOR THREE VALUES OF LIFETIME

effective IF input noise temperature to the available conversion gain. Extensive noise measurements were made as a function of IF frequency, DC bias, and local oscillator power, to determine the mixer-preamplifier combination offering the best combination of sensitivity, frequency response, and power dissipation.

A Ge:Cu mixer element (No. C-1) similar to the one used in the GSFC packaged receiver (reference 2) as well as one with higher (No. C-2) and one with lower (No. C-3) compensation levels were tested up to the 1.5-GHz region.

1. Ge:Cu No. C-1

The previously-measured (reference 8) available G-R noise (quantum noise referred to mixer output) power, as a function of frequency of mixer element C-1 is shown in Figure 3-2 for two values of DC bias power. The method of measurement was described in reference 1. By a substitution technique, the G-R noise output from the mixer element alone is measured directly under operational conditions, with laser local oscillator power applied. This measurement yields the values for τ and μ, since

$$\overline{I_{GR}^2} = \frac{4q\tau\mu B}{L^2 (1 + \omega^2 \tau^2)} P_{DC} \qquad (1)$$

where

$\overline{I_{GR}^2}$ = mean-square G-R noise current,

P_{DC} = dc bias power.

The experimentally-measured G-R noise power rolls off at about 6 db/octave as the above equation predicts, with the 3-db roll-over frequency at approximately 750 MHz, yielding $\tau = 2 \times 10^{-10}$ sec. This 3-db point is called the mixer roll-over frequency, f_{c-m}.

Measurements were made on Mixer No. C-1 integrated with an early-model wideband IF amplifier (Figure 3-3). The methods used give an indirect measurement of receiver (mixer-preamplifier combination) sensitivity as a function of frequency. It is performed by measuring the total noise (G-R noise and thermal noise) relative to thermal noise only, and referring the ratio to an absolute measurement of NEP under low frequency quantum-noise-limited conditions. The receiver roll-over frequency, f_{c-r}, is defined as the frequency where this ratio first achieves the value 2. The reference value, NEP (hereafter called P_{MIN}) was measured to be 7.5×10^{-20} watt/Hz at an IF of 10 kHz. The DC bias power was 135 milliwatts, and the mixer resistance had been reduced to 1000 ohms by the laser local oscillator. These conditions were maintained throughout the frequency run, up to 1.5 GHz.

The results are plotted in Figure 3-2, on both an absolute scale (watt/Hz) and a relative scale indicating the degradation in performance with frequency. The NEP is less than 1.3×10^{-19} watt/Hz from 15 to 800 MHz, less than 2.4×10^{-19} watt/Hz up to 1 GHz and less than 3.6×10^{-19} watt/Hz up to 1.5 GHz. The peaks and valleys in the performance (with this early-model amplifier and matching network) are due to non-optimum high-frequency impedance transformations.

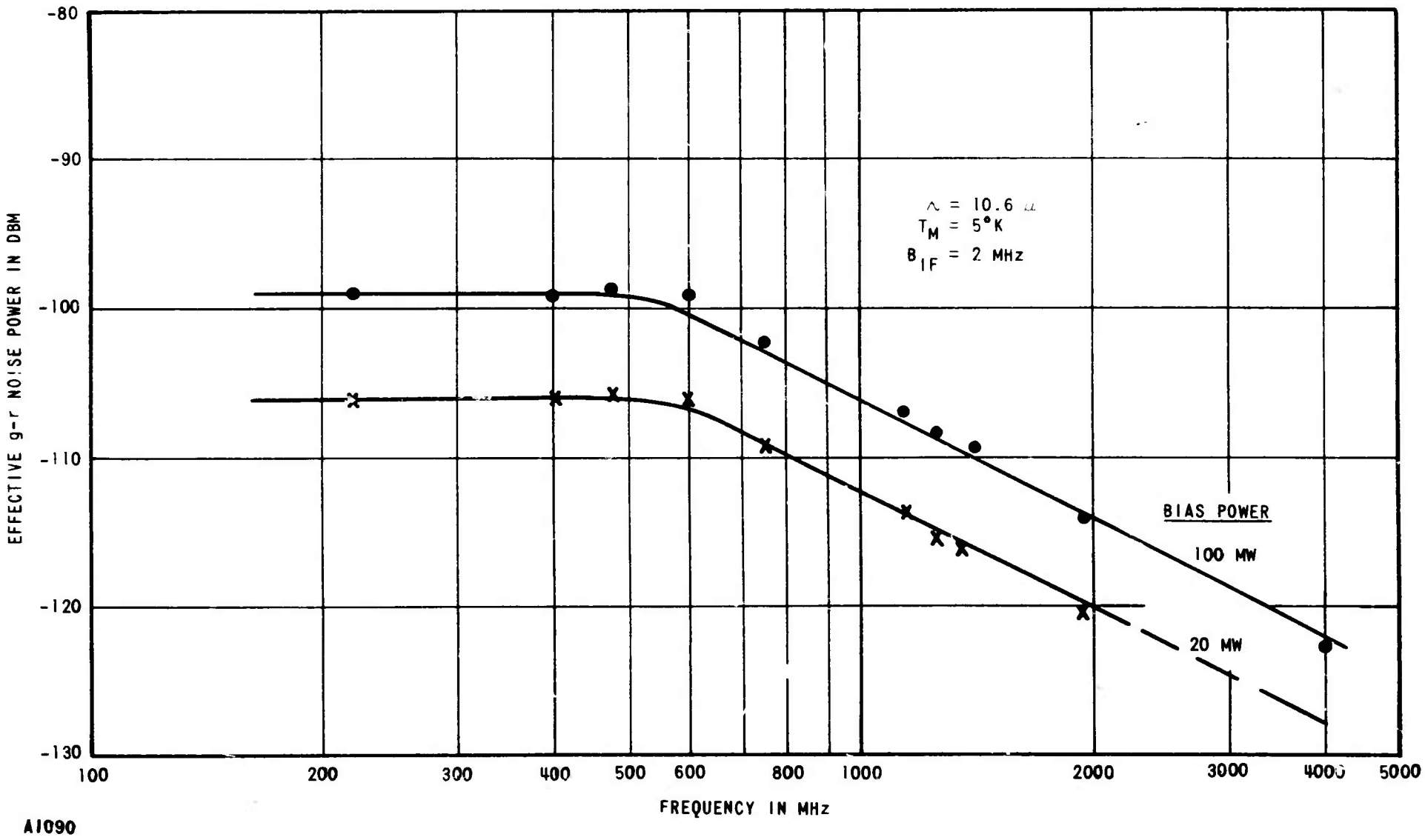

FIGURE 3-2. MEASURED G-R NOISE POWER FOR MIXER No. C-1

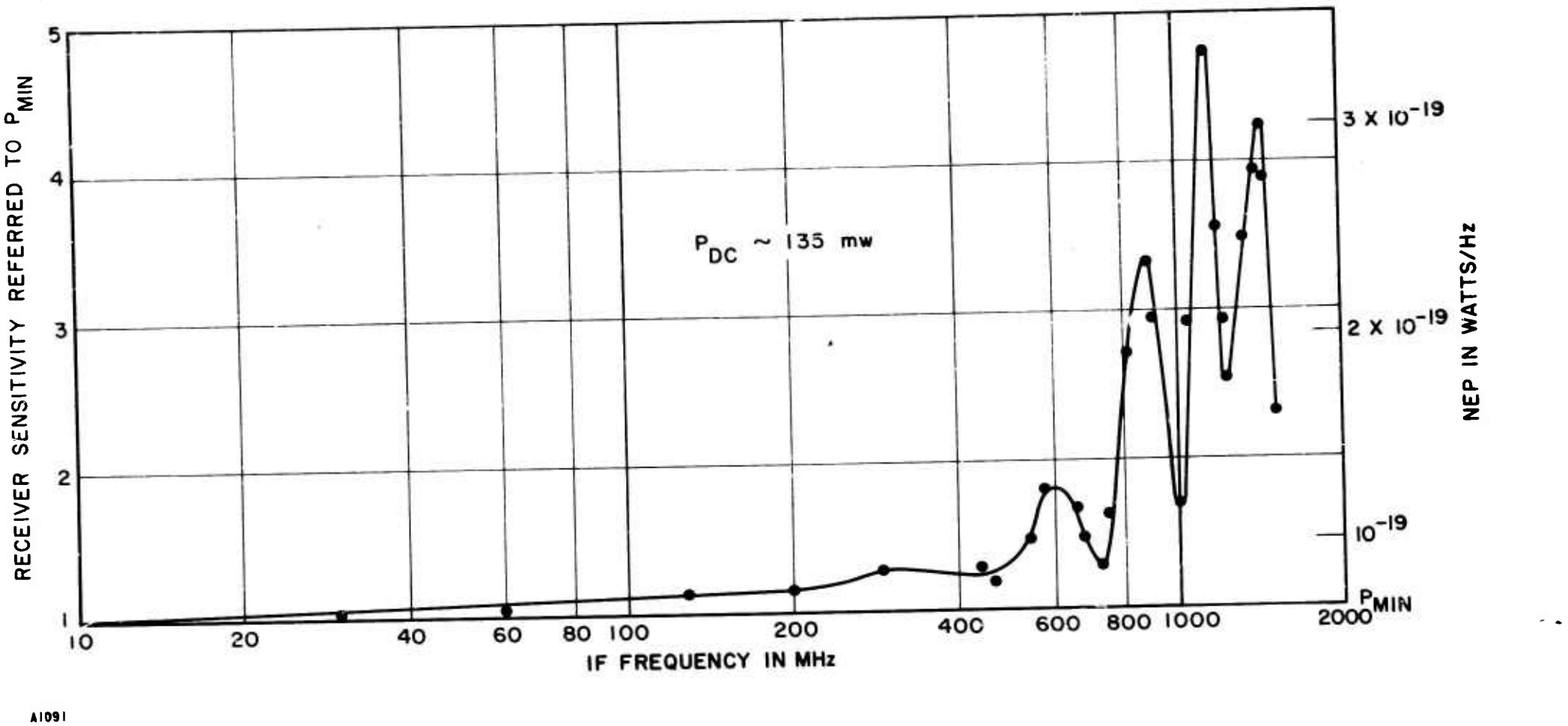

FIGURE 3-3. RECEIVER SENSITIVITY VS IF FREQUENCY FOR Ge:Cu NO. C-1

Figure 3-4 shows another noise ratio measurement with mixer No. C-1, using the improved low-noise amplifier discussed in Section III-G. A substantial sensitivity improvement is evident compared to Figure 3-3. The maximum NEP's inferred from Figure 3-3 are 1.5×10^{-19} and 2.7×10^{-19} watt/Hz (from 10 MHz up to 1.43 GHz) for bias voltages of 15 and 10 volts, respectively, and sufficient LO power to reduce mixer resistance to 2000 ohms. The bias voltages correspond to bias power of 112 and 50 milliwatts, respectively. At present, the IF amplifier operates from 10 MHz to 1.43 GHz, but the upper frequency is expected to be extended beyond 1.5 GHz during the next report period.

The measured conversion gain at 10 kHz was approximately +8 and +10.5 db for the 10- and 15-volt bias conditions.

Receiver roll-over frequencies (fc-r) of 1.43 GHz and 980 MHz were obtained for 15 and 10 volts bias, respectively.

Figure 3-5 shows the I-V characteristics of mixer No. C-1, with various levels of LO power. The mixer resistance is seen to vary from 150,000 ohms to 400 ohms as the applied LO power is increased. Also note the linearity of the curves, since much of the photoconductive mixer analysis is simplified by this assumption.

2. Ge:Cu No. C-2

Figure 3-6 shows a noise-ratio sensitivity measurement on mixer element C-2, using sufficient LO power to reduce the mixer resistance to 2200 ohms and applied DC bias of 10 and 15 volts. Mixer element C-2 has a carrier lifetime that is estimated to be one-half that of mixer No. C-1. This was expected to reduce to one-half the available mixer gain at low IF frequencies, and to roughly double the mixer roll-over frequency to the 1.5-GHz region. As can be seen from Figure 3-5, the receiver roll-over frequencies, that were measured, were 910 MHz (15 volts applied) and 880 MHz (10 volts applied). These correspond to NEP's of 2.25×10^{-19} and 3.75×10^{-19} watt/Hz at bias levels of 15 and 10 volts, respectively.

Comparison of Figures 3-4 and 3-6 shows that mixer No. C-2 yields poorer performance than mixer No. C-1, at an IF near 1.4 GHz for nearly equal mixer resistance and DC bias power values. It is concluded that a mixer element similar to type C-1 will better meet the requirements for the proposed 1.5 GHz array.

At higher IF frequencies, up to 2 GHz, the C-2 mixer element should provide better receiver noise performance. Preliminary measurements of mixer No. C-2 with a laboratory low-noise IF amplifier (1- to 2-GHz passband) resulted in indirectly measured noise-ratio sensitivities of less than 7×10^{-19} watt/Hz (up to 1.8 GHz), and less than 12.6×10^{-19} watt/Hz (up to 2.0 GHz) for a mixer resistance of 3600 ohms, and applied bias of 15 volts. These results could be improved by reducing the mixer impedance (by increasing LO power) and improving the non-optimum IF amplifier.

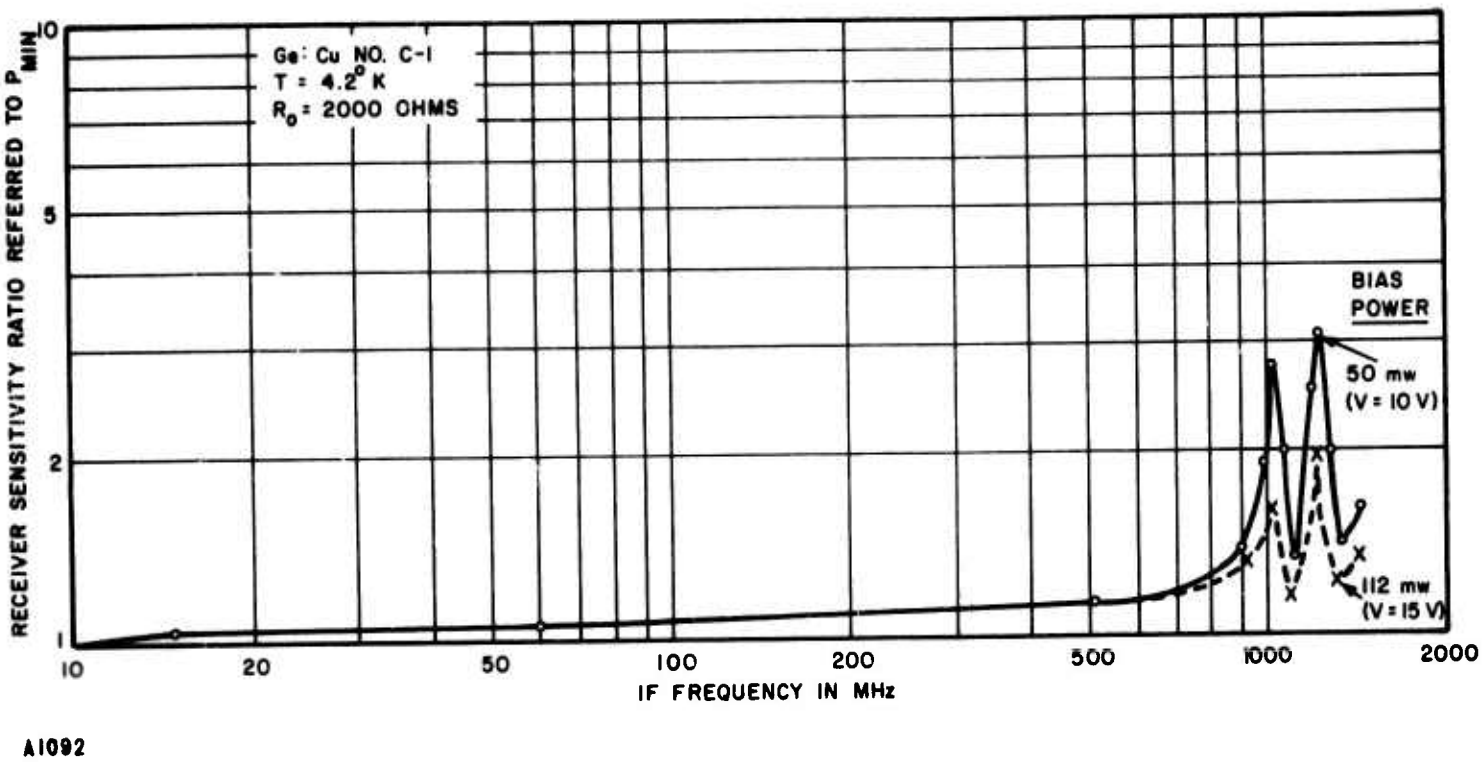

FIGURE 3-4. RECEIVER SENSITIVITY VS IF FREQUENCY FOR Ge:Cu NO. C-1 USING IMPROVED IF AMPLIFIER

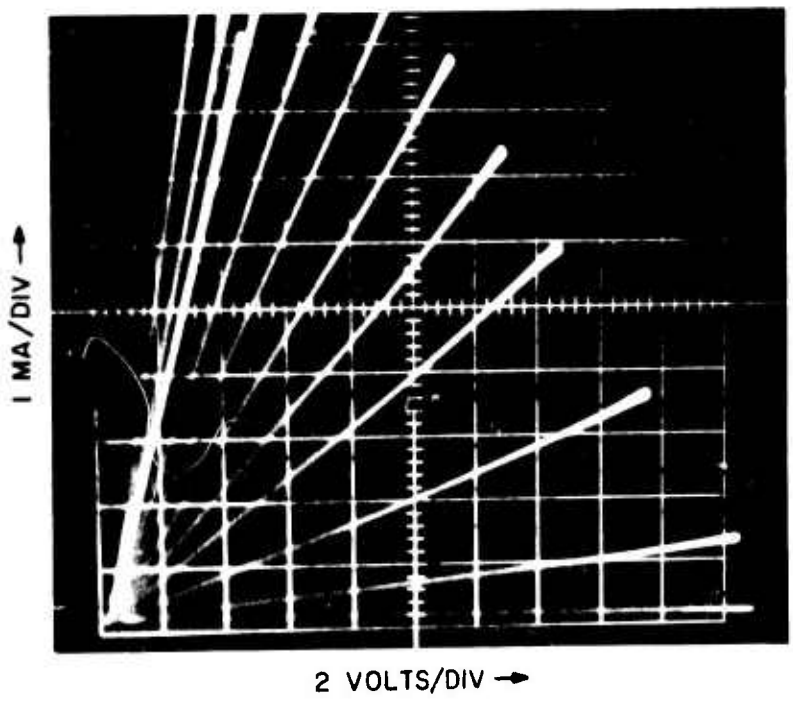

FIGURE 3-5. I-V CHARACTERISTIC OF Ge:Cu NO. C-1 FOR VARIOUS LASER LO POWER LEVELS

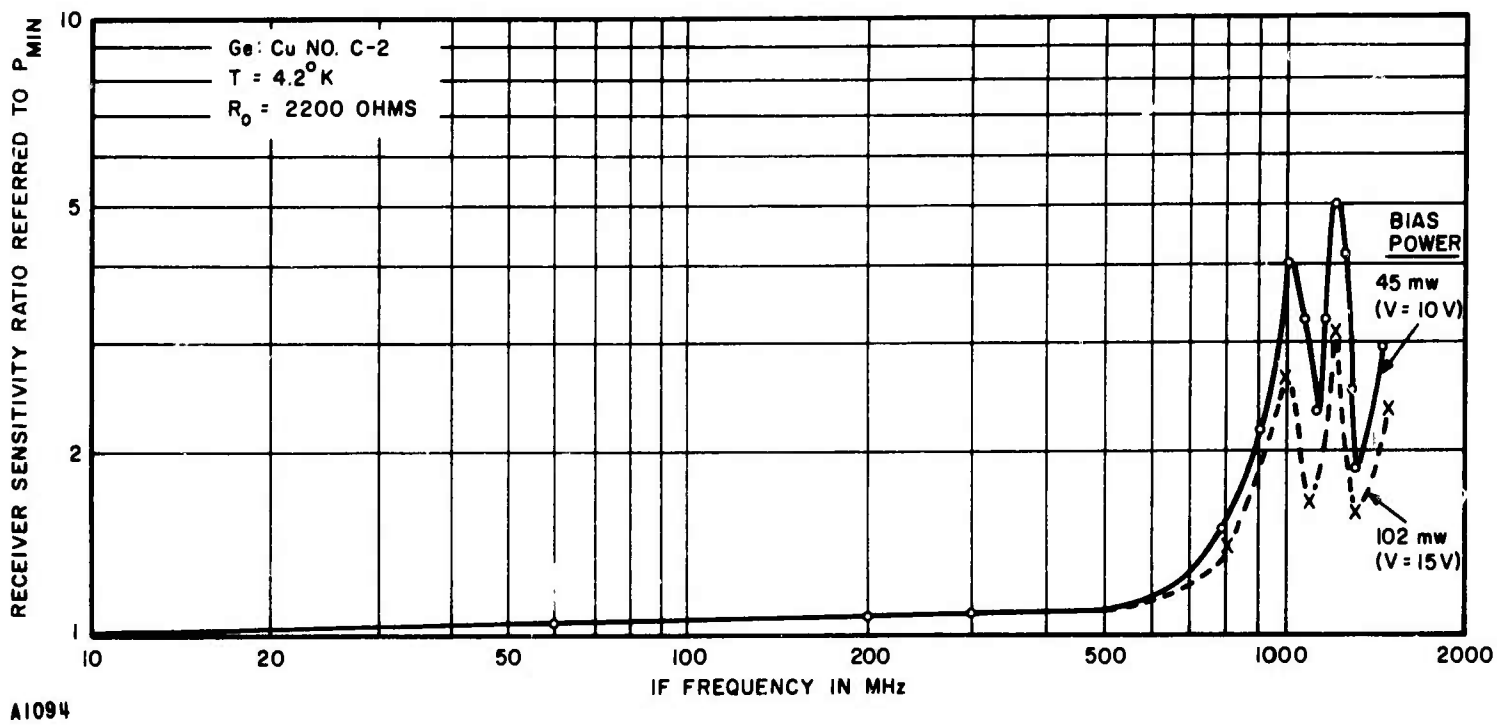

FIGURE 3-6. RECEIVER SENSITIVITY VS IF FREQUENCY FOR Ge:Cu NO. C-2 USING IMPROVED IF AMPLIFIER

3. Ge:Cu No. C-3

The directly measured G-R noise power output of element C-3 is shown in Figure 3-7. This shows that the mixer roll-over frequency is below 400 MHz, as expected.

Noise-ratio sensitivity measurements on mixer element C-3 resulted in poor performance near 1.5 GHz, so that no further measurements were taken.

Further work on copper-doped germanium mixers is in progress to increase high-frequency response, increase sensitivity, and reduce power dissipation requirements without degrading the overall sensitivity at 1.5 GHz.

E. MERCURY-DOPED GERMANIUM

Sensitivity and frequency response measurements were made on a partially-compensated mercury-doped germanium mixer element cooled to 4.2°K. The Ge:Hg element is useful from approximately 9 to 13 microns. The indirectly measured noise-ratio sensitivity as a function of IF frequency is shown in Figure 3-8 for an applied LO power sufficient to reduce mixer resistance to 3000 ohms, and a bias voltage of 15 volts. It was concluded, from the degraded low-frequency sensitivity and the low receiver roll-over frequency, that this mixer element is not suitable for a 1.5 GHz receiver.

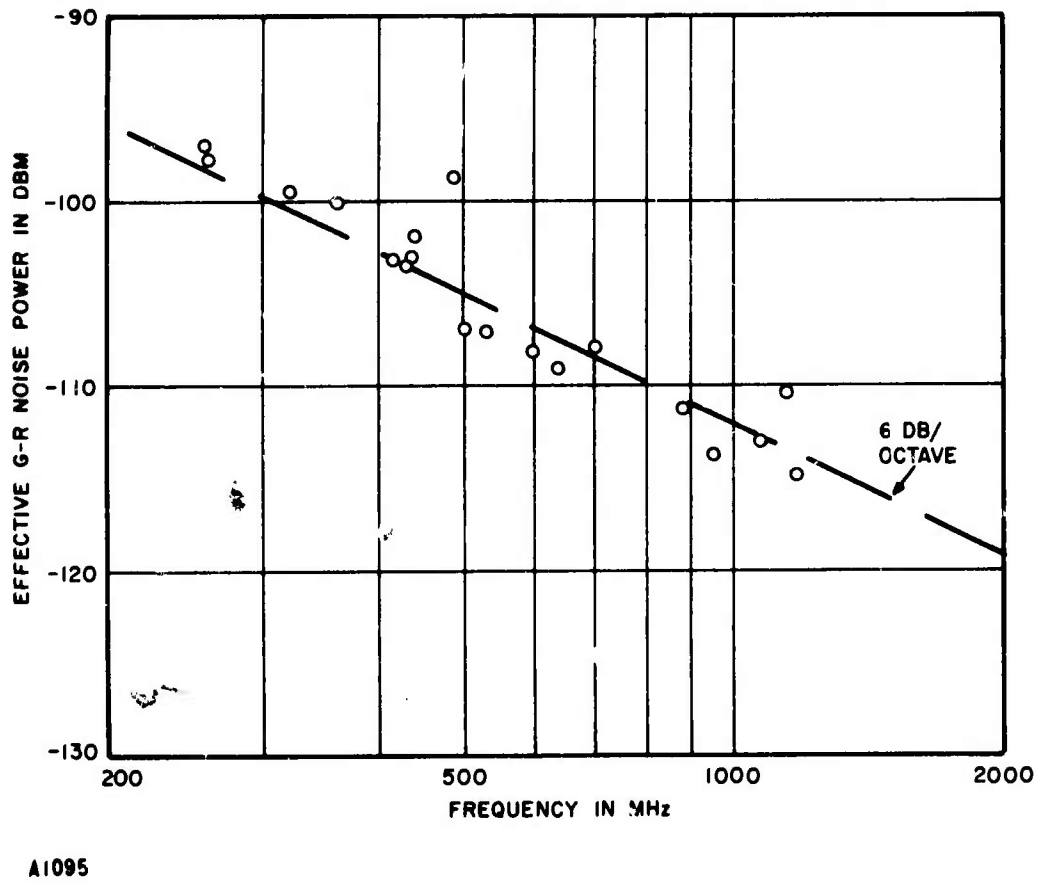

FIGURE 3-7. MEASURED G-R NOISE POWER VS IF FREQUENCY FOR Ge:Cu NO. C-3

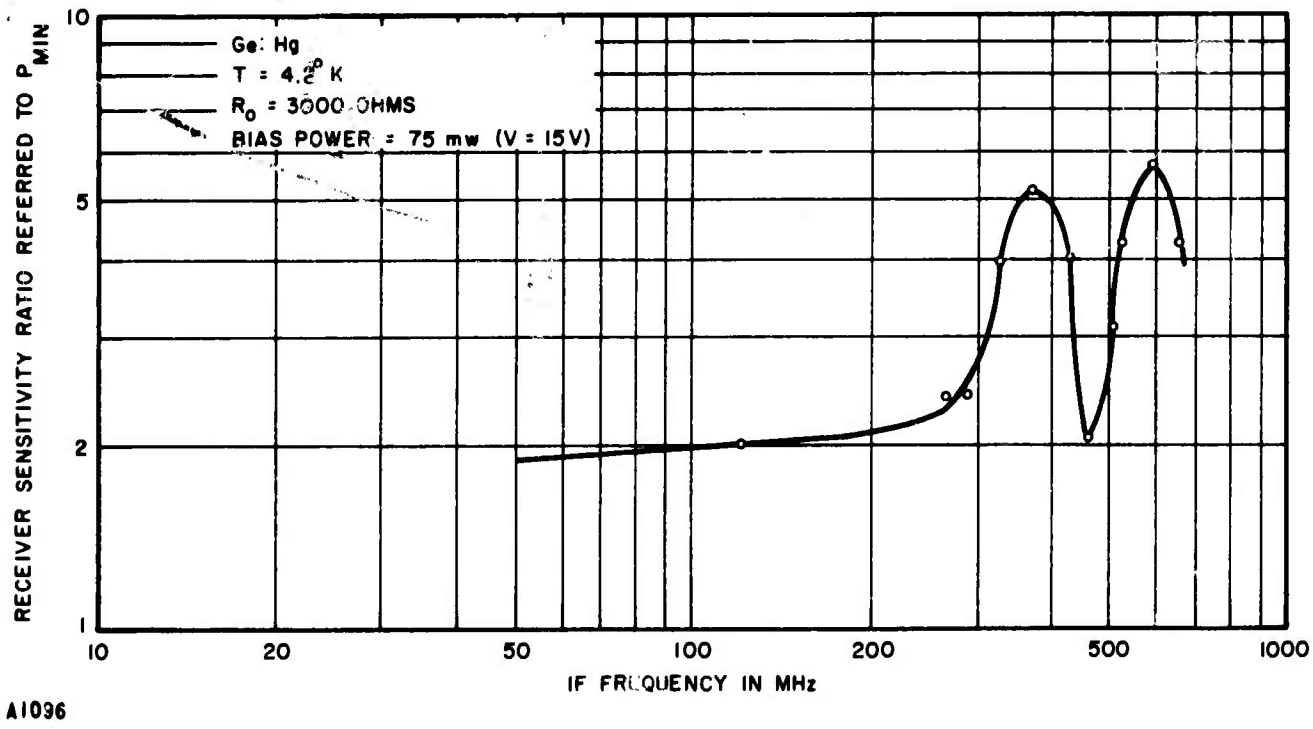

FIGURE 3-8. RECEIVER SENSITIVITY FOR Ge:Hg MIXER

F. ALUMINUM-DOPED SILICON

Sensitivity and frequency response measurements were made on one aluminum-doped silicon detector element previously investigated by Soref (reference 12). The element had an estimated $\tau = 5 \times 10^{-10}$ sec (according to Soref) and was deemed to be low enough to be of possible use to this program. The indirectly-measured noise-ratio sensitivity, as a function of IF frequency, is shown in Figure 3-9 for an applied LO power sufficient to reduce the mixer resistance to 550 ohms, and a DC bias voltage of 10 volts. The receiver roll-over frequency occurs at approximately 325 MHz. At this writing, it has not been established whether this relatively low value is due to a long carrier lifetime or the large interelectrode capacitance of the nonoptimum element geometry. In any event, this element is not deemed suitable for 1.5 GHz operation.

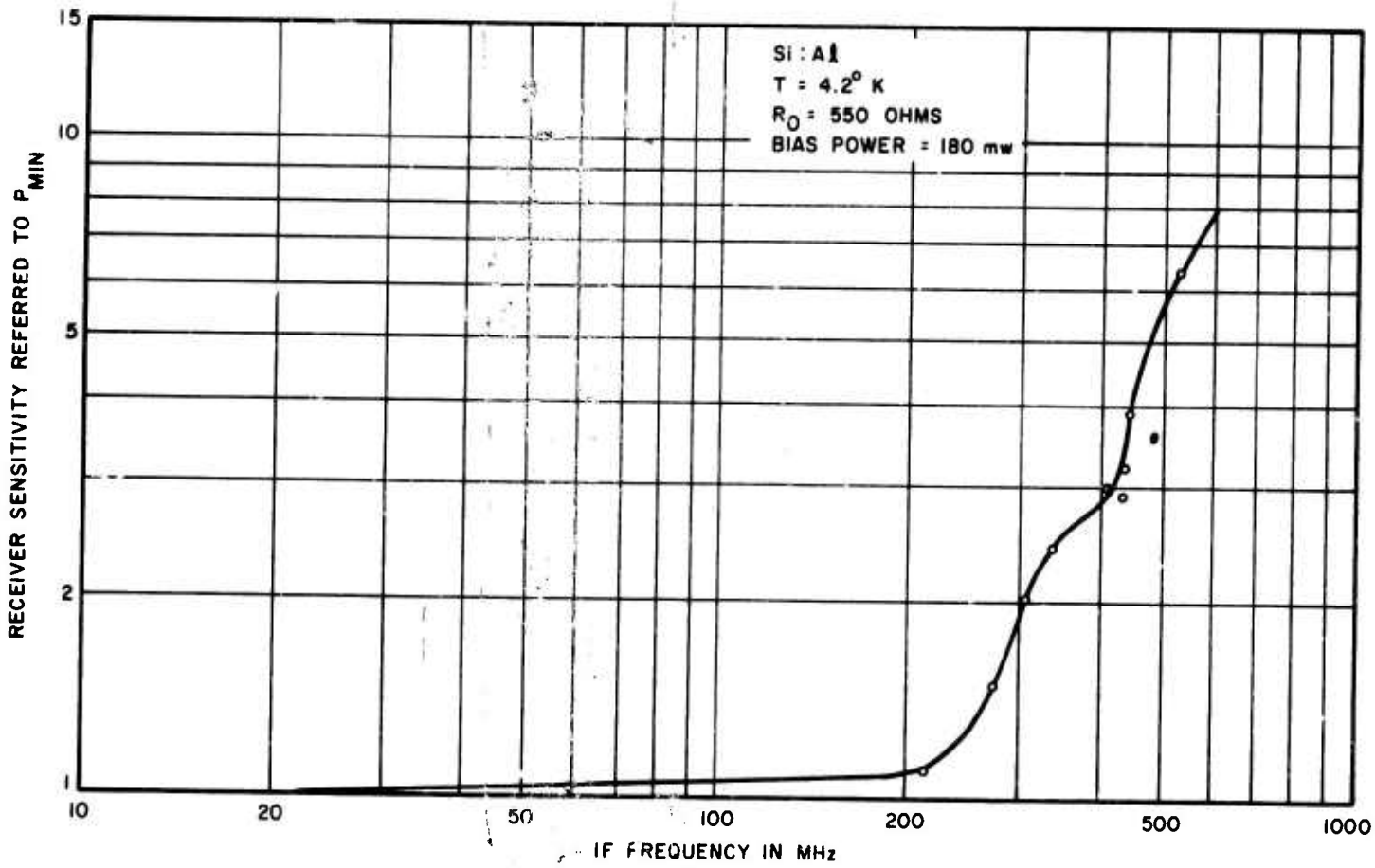

FIGURE 3-9. RECEIVER SENSITIVITY FOR Si:Al MIXER

G. MERCURY-CADMIUM TELLURIDE

Photoconductive (PC) and photovoltaic (PV) HgCdTe mixer elements have been investigated to determine their potential usefulness on this program. Analysis of PC mixer operation has been previously reported (reference 1). A comparable analysis of a PV mixer has been carried out and is given in detail in Section IV. This analysis considered conversion gain, NEP, and IF bandwidth in terms of engineering parameters such as diode capacitance, series resistance, shunt conductance, and LO power. (The use of double- and triple-tuned circuits to extend the high frequency response is also considered.) The analysis uses the same conversion gain approach successfully used in the PC mixer analysis. To date, sub-nanosecond response times have not been reported for HgCdTe detectors.

1. PHOTOCONDUCTIVE OPERATION

Figure 3-10 shows the measured G-R noise output power, as a function of DC bias power, of an experimental photoconductive HgCdTe mixer element, cooled to 77°K. The measurement technique is essentially similar to the one previously used to evaluate germanium detectors. As predicted by the photoconductive analysis, the G-R noise power is directly proportional to bias power and drops off at the higher frequencies.

Figure 3-11 gives the measured G-R noise power, as a function of IF frequency. The mixer roll-off frequency was too low to be accurately determined with the measurement technique that was employed, and hence is of no interest for the 1.5 GHz application. Preliminary tests on other HgCdTe mixers indicate 3-db roll-off frequencies beyond 100 MHz.

Figure 3-12 shows the variation of the I-V characteristic of the HgCdTe mixer with LO power. (The mixer resistance is seen to vary from 400 to 20 ohms when LO power is applied.)

The above element, with an estimated carrier lifetime of 1.3 nanoseconds, is faster than any previously reported HgCdTe detector.

Preliminary tests on other HgCdTe mixers indicate 3-db roll-off frequencies beyond 100 MHz.

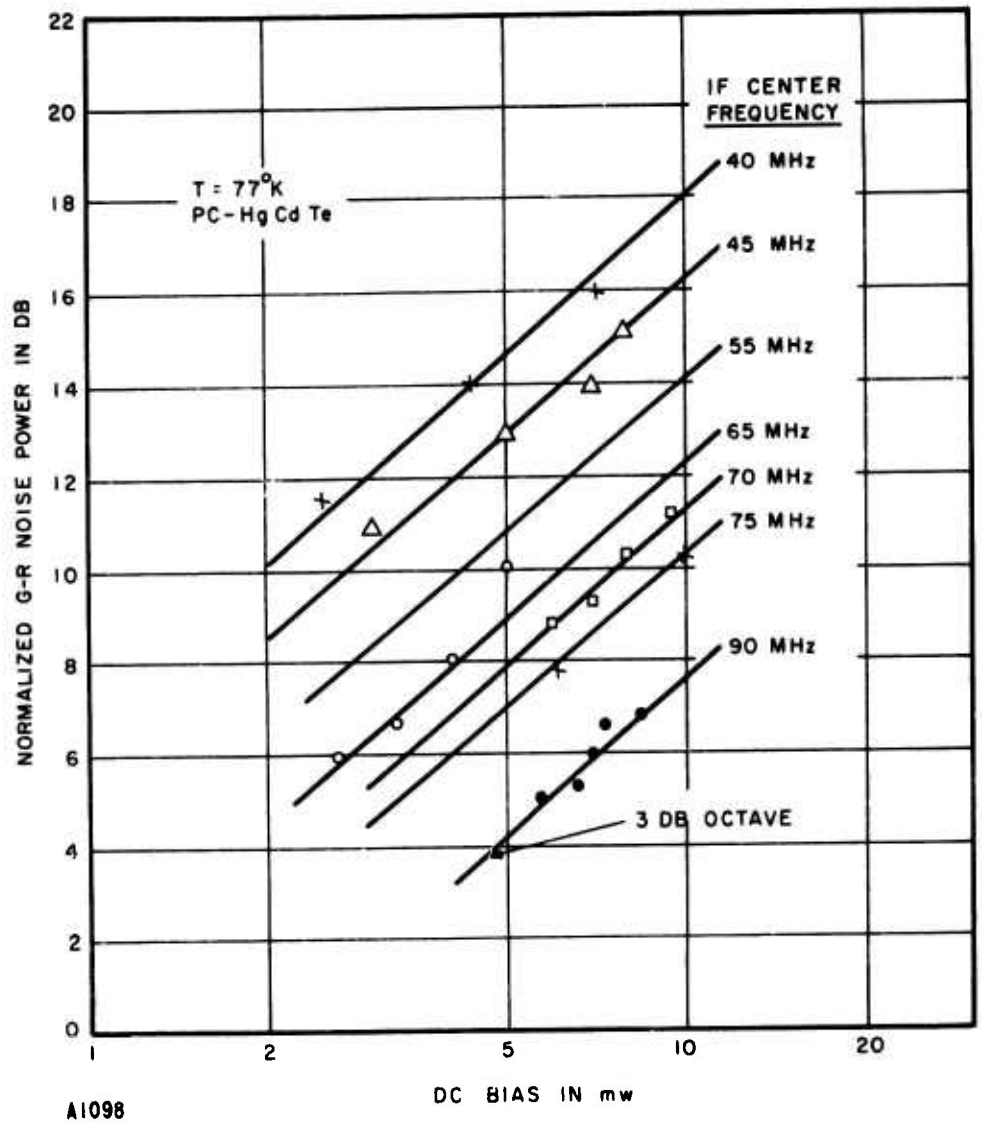

FIGURE 3-10. MEASURED G-R NOISE AS A FUNCTION OF BIAS POWER FOR HgCdTe MIXER

H. IF AMPLIFIER

A prime objective of the amplifier design is the achievement of low-noise, flat gain, and uniform input impedance broadband over the entire 10-MHz to 1.5-GHz band, in a single amplifier. Starting with an earlier 1-GHz amplifier design (reference 2) several modifications have been tried. Results on the latest model are given below.

With the amplifier driven from a 50 ohm source, its gain was measured as a function of frequency and is given in Figure 3-13. The net gain is 38 db in midband, and over 30 db from 8 MHz to 1.4 GHz.

The measured noise-factor of the amplifier is given in Figure 3-14. The mid-band value is 4.9 db, increases to 6 db at 1.1 GHz, and becomes 7.4 db at 1.4 GHz. Work is still in progress to extend the amplifier performance sufficiently beyond 1.5 GHz to assure satisfactory performance throughout the specified mixer operating band.

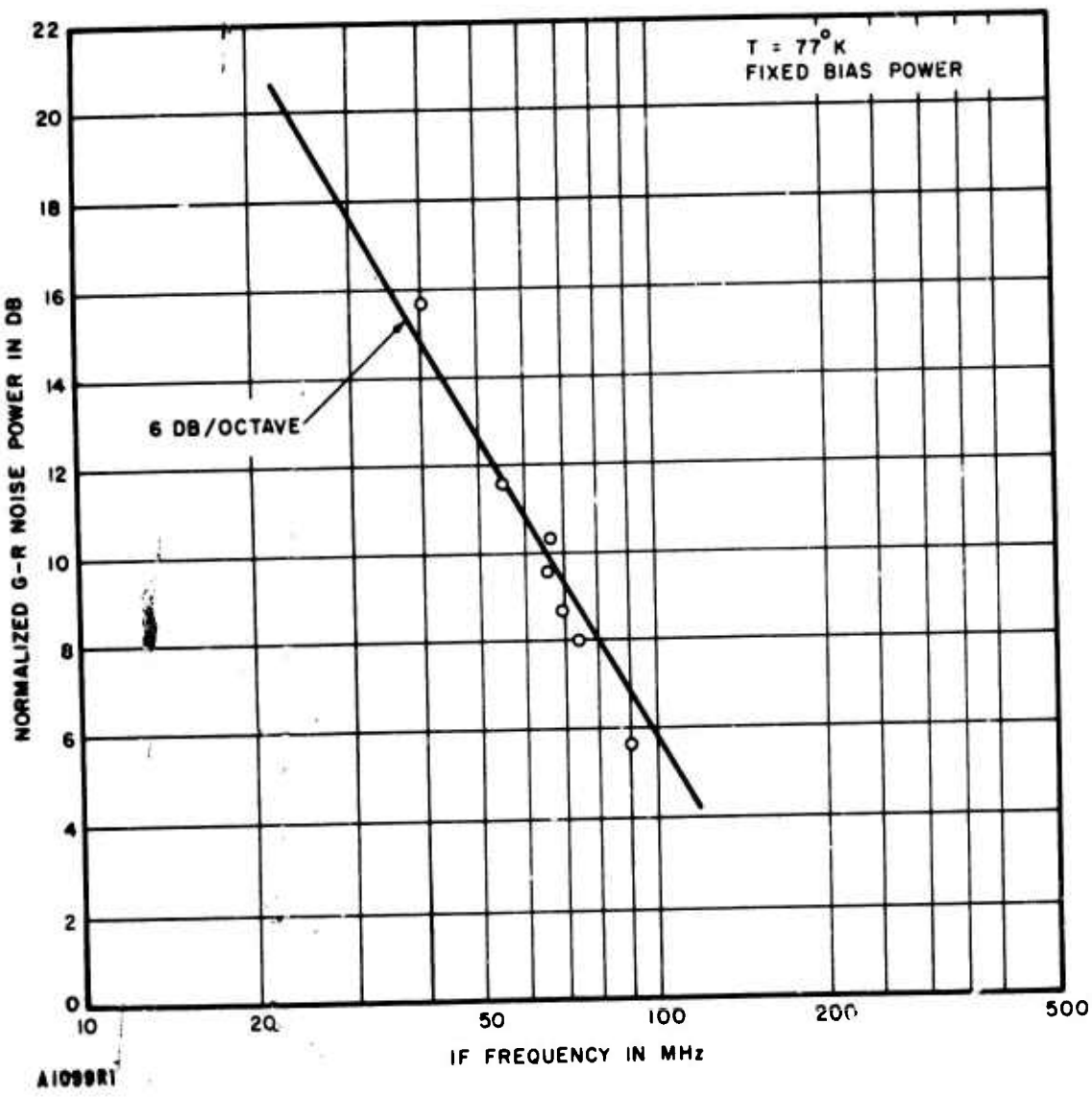

FIGURE 3-11. MEASURED G-R NOISE POWER FOR HgCdTe DETECTOR

This amplifier has been used in the evaluation of most of the mixer elements reported above and operated satisfactorily. A very useful feature of the amplifier is a matching transformer at its input that permits the introduction of DC bias to the mixer element without the need for a broadband bias tee external to it. This transformer also provides a means for obtaining a better impedance match with the mixer element. Work in this area is continuing.

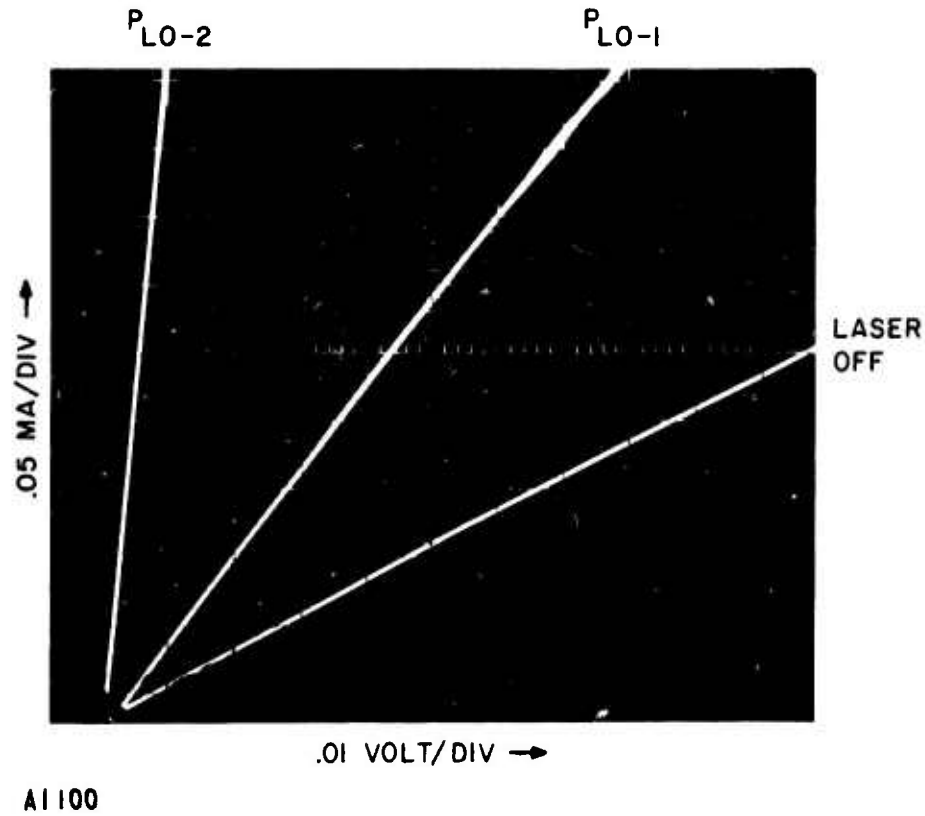

FIGURE 3-12. VARIATIONS OF RESISTANCE WITH LO POWER OF HgCdTe MIXER

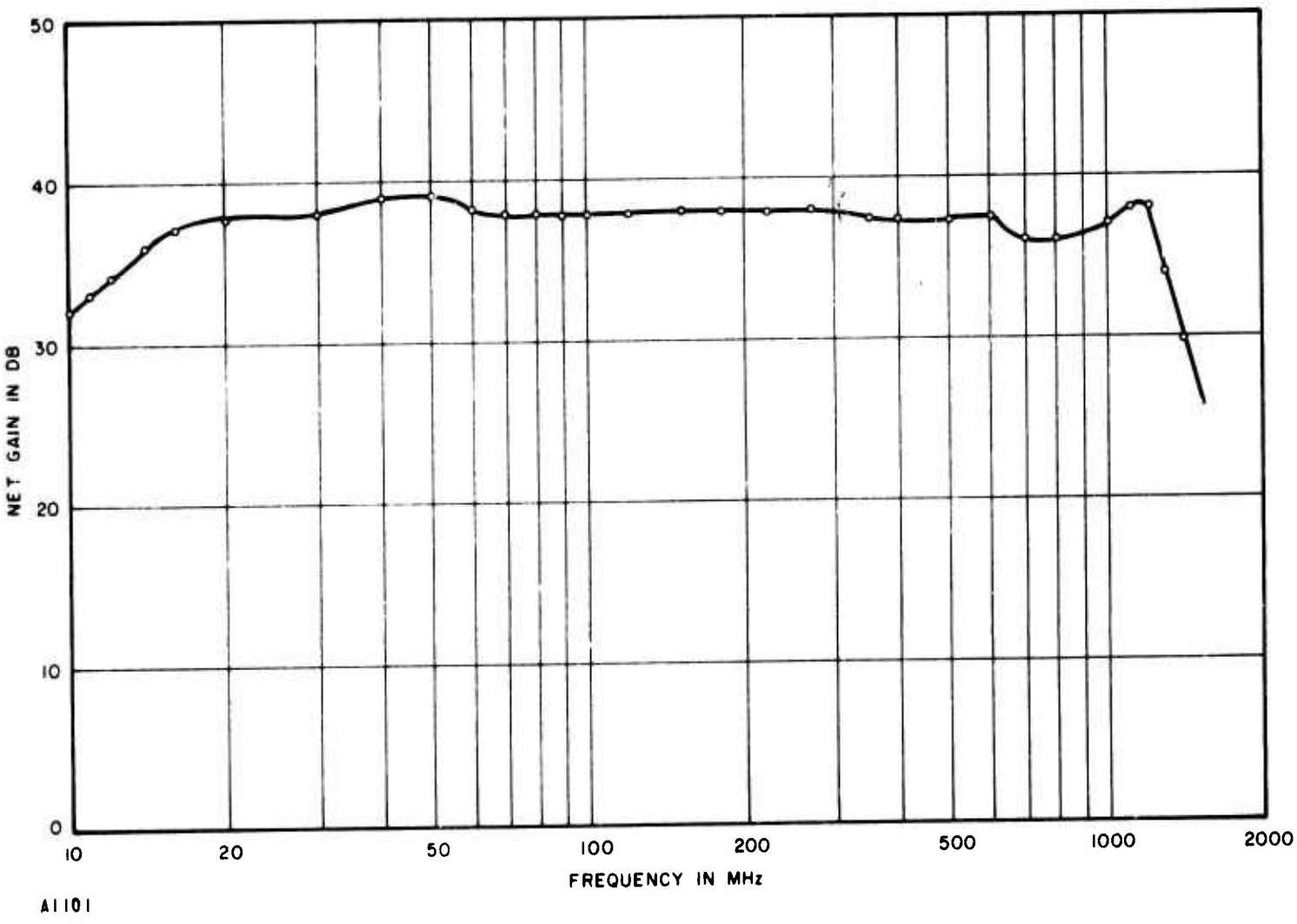

FIGURE 3-13. MEASURED NET GAIN OF WIDEBAND IF AMPLIFIER OPERATING FROM 50-OHM SOURCE RESISTANCE

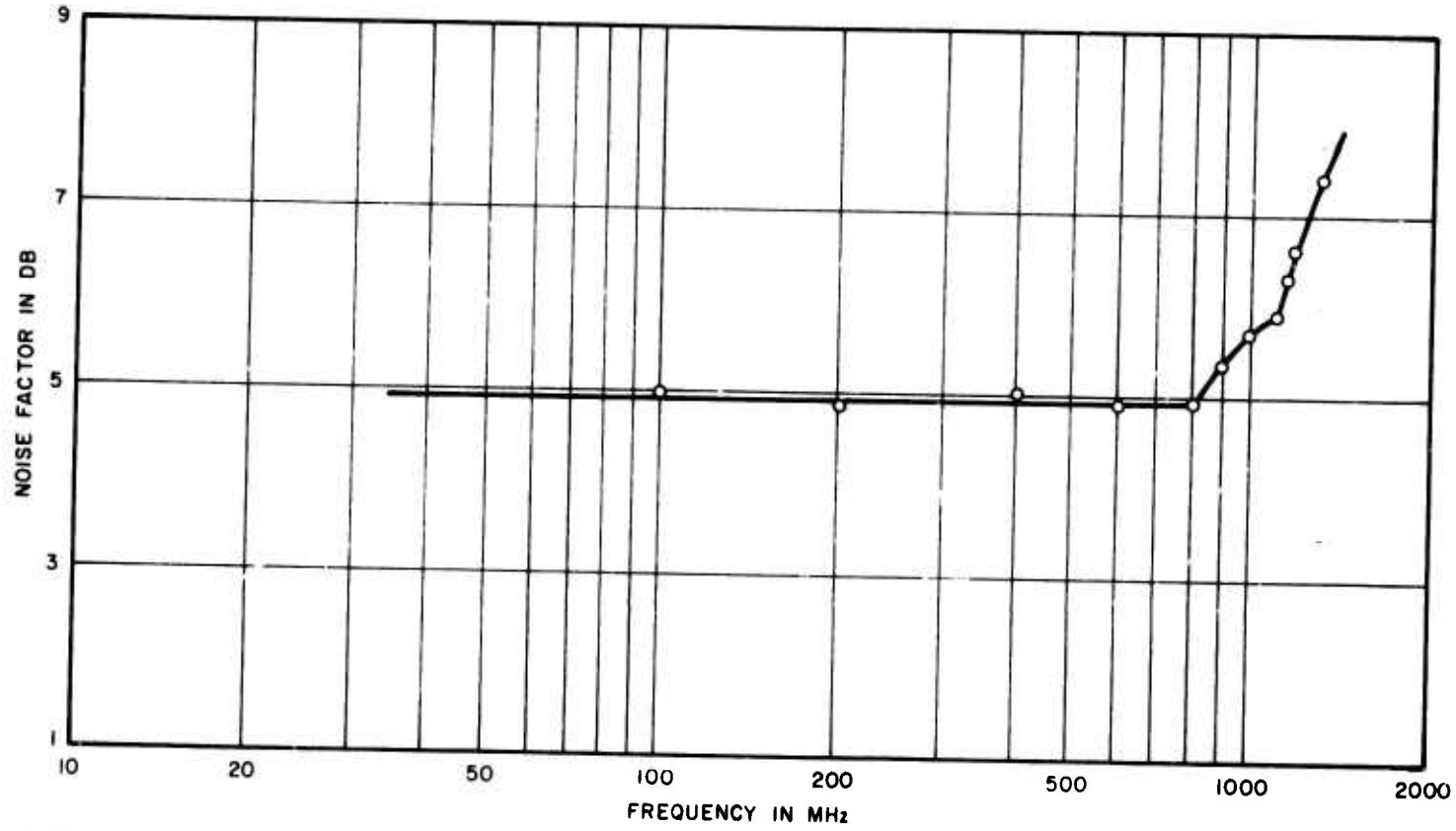

FIGURE 3-14. MEASURED NOISE FACTOR OF WIDEBAND IF AMPLIFIER OPERATING FROM 50-OHM SOURCE RESISTANCE

BLANK PAGE

IV. INFRARED PHOTOVOLTAIC MIXER ANALYSIS

A. INTRODUCTION

An analysis was carried out on the noise equivalent power and IF frequency bandwidth of infrared photovoltaic mixers, with emphasis on 10.6 micron mixing (in such diodes as PV-HgCdTe). Various formulas scattered throughout the literature (references 13 and 14) have been modified to obtain explicit formulas for mixer conversion gain, noise equivalent power (NEP) and IF bandwidth, in terms of such parameters as photodiode capacitance, shunt and series resistance, local oscillator power, etc. The use of double- and triple-tuned circuits to extend the high-frequency response was also investigated. The analysis employs the same conversion gain approach successfully used in the analysis of photoconductive mixers. The objective of the analysis was to gain insight into the potential of 1.5 GHz PV-mixer operation.

B. AVAILABLE IF SIGNAL POWER

The equivalent circuit at IF frequencies for a photovoltaic (PV) infrared mixer is shown in Figure 4-1. The mixer analysis assumes a non-zero leakage conductance and neglects any lead inductance which may be present.

The square of the peak IF signal current is given by

$$\left|I_S^2\right| = 4\left(\frac{\eta q}{h\nu}\right)^2 P_{sig}\, P_{LO}$$

where

I_S = peak IF signal current

ν = signal frequency

η = quantum efficiency

P_{sig} = signal power

P_{LO} = LO power $> P_{sig}$

From Figure 4-1, the ratio of the short circuit current to the signal current is given by:

$$\frac{I_{SC}}{I_S} = \frac{1}{\left(1 + G_D R_S\right) + j\,\omega\, C_D R_S}$$

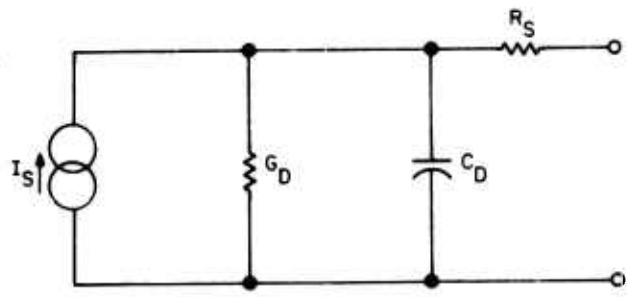

A. BASIC CIRCUIT

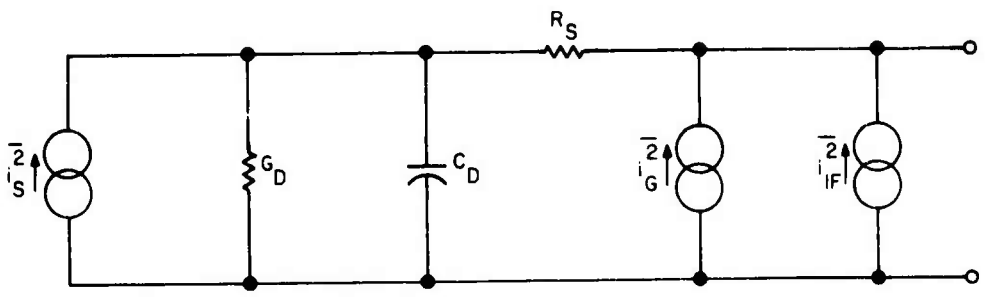

B. INCLUDING NOISE GENERATORS

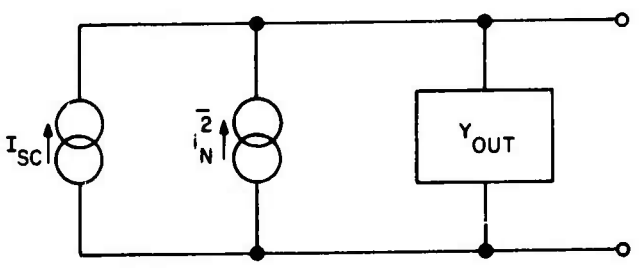

C. NORTON EQUIVALENT

A1103

FIGURE 4-1. EQUIVALENT CIRCUIT FOR INFRARED PHOTOVOLTAIC MIXER

where

I_{SC} = short circuit current

G_D = small signal shunt conductance (slope of I - V curve)

R_S = series resistance

C_D = shunt capacitance

The mixer output admittance can be expressed as:

$$Y_{out} = \frac{G_D + R_S\left(G_D^2 + \omega^2 C_D^2\right) + j\,\omega\, C_D}{\left(1 + G_D R_S\right)^2 + \omega^2 C_D^2 R_S^2}$$

The real component of the output admittance is given by:

$$G'_{out} = \frac{G_D + R_S\left(G_D^2 + \omega^2 C_D^2\right)}{\left(1 + G_D R_S\right)^2 + \left(f/f_c\right)^2}$$

where the cutoff frequency f_c is defined as

$$f_c = \frac{1}{2\pi R_S C_D}$$

For most photovoltaic mixer elements $G_D R_s << 1$, so that

$$G'_{out} \approx \frac{G_D + \omega^2 C_D^2 R_S}{1 + \left(f/f_c\right)^2}$$

The short-circuit current is:

$$\left|I_{SC}\right|^2 = \frac{\left|I_S\right|^2}{\left(1 + G_D R_S\right)^2 + \left(f/f_c\right)^2}$$

and the available output power from the photovoltaic mixer is:

$$\left(P_{IF}\right)_{\text{available}} = \frac{\left|I_{SC}\right|^2}{8\, G'_{out}} = \frac{\left|I_S\right|^2}{8\left[G_D\left(1 + G_D R_S\right) + \omega^2 R_S C_D^2\right]}$$

The output power is 3 db down at an IF frequency given by:

$$f_c' = \frac{\left(1 + R_S G_D\right)^{1/2}}{2\pi C_D \left(R_S / G_D\right)^{1/2}} \approx \frac{1}{2\pi C_D \left(R_S / G_D\right)^{1/2}}$$

C. NOISE

The equivalent noise circuit for the photovoltaic mixing case including noise generators is shown in Figure 4-2. The overall mean-square noise current generator is given by:

$$\overline{i_N^2} = \overline{i_G^2} + \overline{i_{IF}^2} + \frac{\overline{i_S^2}}{\left(1 + G_S R_S\right)^2 + \left(f/f_c\right)^2}$$

where

$\overline{i_G^2}$ = thermal noise = $4R T_m B G_{out}'$

$\overline{i_{IF}^2}$ = IF amplifier noise = $4R T_{IF}' B G_{out}'$

$\overline{i_S^2}$ = shot noise $\approx 2q I_o B$ for condition $f_{IF} < 1/(8T_r)$ (reference 15)

k = Boltzmann's constant

T_m = physical temperature of mixer

B = IF bandwidth

T_{IF}' = effective input noise temperature of IF amplifier which is a function of its source impedance

I_o = DC photocurrent

T_r = carrier transit time

D. MIXER GAIN

The available photovoltaic mixing gain--that is, the ratio of the available IF output power to the available infrared signal power, is given by:

$$G = \frac{P_{IF\ (available)}}{P_{sig}} = \frac{\left|I_S\right|^2}{8 P_{sig} \left[G_D \left(1 + G_D R_S\right) + \omega^2 R_S C_d^2\right]}$$

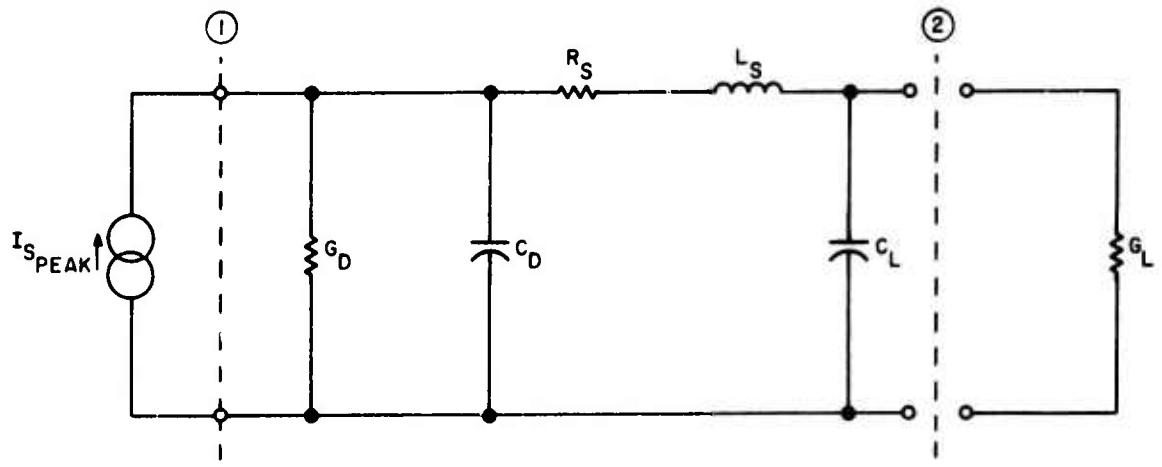

FIGURE 4-2. EQUIVALENT CIRCUIT FOR TUNED PHOTOVOLTAIC MIXER

which can be written as

$$G = \frac{\left(\frac{\eta q}{h\nu}\right)^2 P_{LO}}{2\left[G_D\left(1 + G_D R_S\right) + \omega^2 R_S C_d^{\,2}\right]}$$

For photovoltaic mixer $\tau/T_r = 1$. Therefore (reference 1), under the condition that, $P_{LO} >> P_{sig}$, the DC photocurrent is given by:

$$I_o = \frac{\eta q}{h\nu}\left(\frac{\tau}{T_r}\right) P_{LO} = \frac{q}{h\nu}\,\eta\, P_{LO}$$

Combining these equations:

$$G = \frac{\eta q I_o}{2h\nu} \frac{1}{G_D\left(1 + R_S G_D\right) + \omega^2 R_S C_D^{\,2}}$$

and for $R_S G_D << 1$

$$G \approx \frac{\eta q I_o}{2\, h\nu\, G_D} \frac{1}{1 + \left(f/f_c\right)^2}$$

From this, is seen that the available conversion gain is 3-db down at an IF frequency $\left|f_c'\right|$ defined above.

It is interesting to note that the conversion gain varies with LO power through its effect on the photocurrent, I_o.

E. SIGNAL-TO-NOISE RATIO

The signal-to-noise ratio for the photovoltaic mixer is:

$$\frac{S}{N} = \frac{\left|I_{SC}\right|^2}{2\,\overline{i_N^2}}$$

Substituting expressions for the noise current and the short circuit current given:

$$\frac{S}{N} = \frac{\left|I_S\right|^2}{8k\left(T_m + T_{IF}'\right) B\left[G_D + R_S\left(G_D^2 + \omega^2 C_D^2\right)\right] + 4qI_oB}$$

$$= \frac{\left(\frac{\eta q}{h\nu}\right) P_{sig}\, I_o}{I_o qB + 2k\left(T_m + T_{IF}'\right) B\left[G_D\left(1 + R_S G_D\right) + \omega^2 R_S C_D^2\right]}$$

Thus, the noise equivalent power (NEP); that is, the value of signal power to give an IF signal-to-noise ratio equal to unity, is:

$$NEP = \frac{h\nu B}{\eta}\left\{1 + \frac{2k\left(T_m + T_{IF}'\right)}{qI_o}\left[G_D\left(1 + R_S G_D\right) + \omega^2 R_S C_D^2\right]\right\}$$

This is reducible to:

$$NEP = \frac{h\nu B}{\eta} + \frac{k\left(T_m + T_{IF}'\right) B}{G}$$

which is the same expression as that derived for the photoconductive mixing case, with the exception of the factor of two in the quantum noise term due to the generation recombination noise in photoconductors. Moreover, there are differences in the expressions for G, the conversion gain, between photovoltaic and photoconductive mixing.

F. QUANTUM NOISE FACTOR

The quantum noise factor is defined as the noise equivalent power divided by the fundamental limiting quantum power ($h\nu B$):

$$QF = \frac{1}{\eta}\left[1 + \frac{R\left(T_m + T_{IF}'\right)}{h\nu\, G}\right]$$

G. BROADBANDING USING MAXIMALLY FLAT TUNING

Using the equivalent circuit for the tuned photovoltaic mixer shown in Figure 4-2, a broadbanding analysis was carried out to determine the values of L_S and C_L required for maximally-flat IF frequency response. The results for single, double, and triple tuned response are summarized in Table II using values for G_D, R_S, and C_D which are considered representative for available PV mixers and a R_L of 50 ohms. From Table II, the 3-db cut-off frequency improved from 153 to 174 MHz when the single-tuned response is changed to a triple-tuned response.

The transducer gain is defined as the actual power delivered to the load, divided by the available infrared signal power, for a real load G_L. It is given by:

$$G_T = 2\left|\frac{V_2}{I_S}\right|^2\left(\frac{\eta q}{h\nu}\right)^2 G_L\, P_{LO}$$

where V_2 and I_S are peak values. For the single-, double-, and triple-tuned maximally-flat response tranducer gain is given by:

$$N = 1 \qquad G_T = \frac{2\, G_L \left(\eta q/h\nu\right)^2 P_{LO}}{\left(G_D + G_L + R_S\, G_D\, G_L\right)^2 + \omega^2\, C_D^2\left(1 + R_S\, G_L\right)^2}$$

$$N = 2 \qquad G_T = \frac{2\, G_L \left(\eta q/h\nu\right)^2 P_{LO}}{\left(G_D + G_L + R_S\, G_D\, G_L\right)^2 + \left(L_S\, C_D G_L\right)^2 \omega^4}$$

$$N = 3 \qquad G_T = \frac{2\, G_L \left(\eta q/h\nu\right)^2 P_{LO}}{\left(G_D + G_L + R_S\, G_D\, G_L\right)^2 + \left(L_S\, C_D C_L\right)^2 \omega^6}$$

or, in general,

$$G_T = \frac{M}{1 + \left(f/f_{c_N}\right)^{2N}}$$

TABLE II. SUMMARY OF CALCULATED DATA FOR MAXIMALLY FLAT RESPONSE IN PHOTOVOLTAIC MIXER ELEMENTS

Number of Elements	$2\pi f_c$	Roll-Off	L_S* (nanohenries)	C_L* (picofarads)	f_c* MH_z
1	$\frac{1}{C_D}\left(G_D + \frac{G_L}{1 + R_S G_L}\right)$	6 db/octave	0	0	153
2	$\left[\frac{G_D + G_L\left(1 + R_S G_D\right)}{L_S C_D G_L}\right]^{1/2}$	12 db/octave	45.6	0	169
3	$\left[\frac{G_D + G_L\left(1 + R_S G_D\right)}{L_S C_D C_L}\right]^{1/3}$	18 db/octave	71.8	10.9	174

* Calculated $G_D = 10^{-2}$ mhos, $R_S = 3$ ohms, $C_D = 30$ picofarads, $G_L = 2 \times 10^{-2}$ mhos.

where M is defined as $2G_L (\eta q/h\nu)^2 P_{LO}$. The junction capacitance C_D and shunt conductance G_D vary with detector area and bias voltage.

For N = 1, the optimum G_L for maximum transducer gain is given by:

$$G_{L_{optimum}} = \left[\frac{G_D^2 + \omega^2 C_d^2}{(1 + R_S G_D)^2 + \omega^2 C_D^2 R_S^2} \right]^{1/2}$$

A calculated plot of transducer gain versus frequency, with load conductance G_L as a parameter, is shown in Figure 4-3, using values for G_D, R_S, and C_D that are representative for PV mixer elements. As can be seen from this figure, the available mixer gain is down only 22 db from the peak valve at an IF of 1000 MHz for a load resistance of 50 ohms $G_L = 2 \times 10^{-2}$ mhos

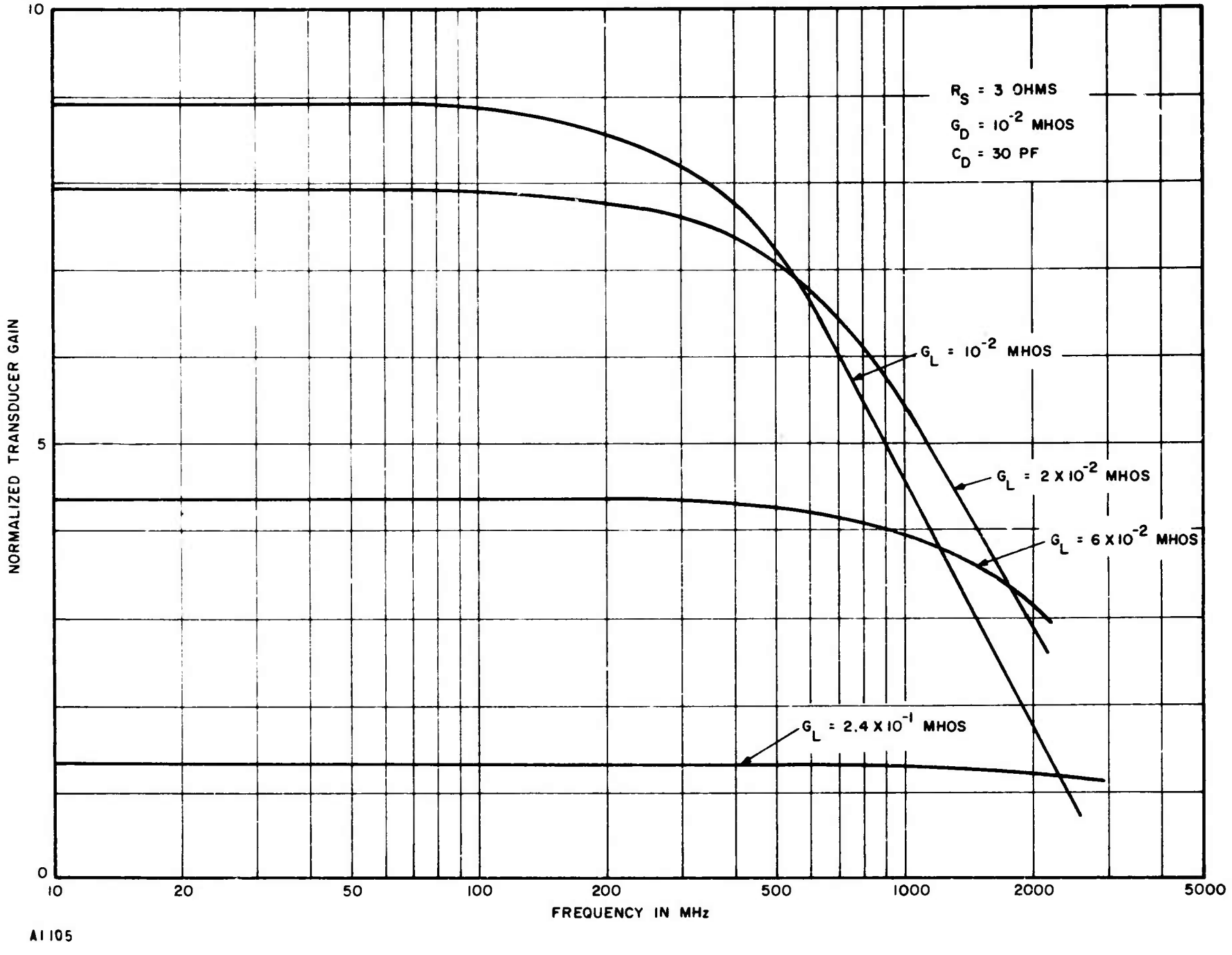

FIGURE 4-3. CALCULATED TRANSDUCER GAIN VS FREQUENCY FOR A PHOTOVOLTAIC INFRARED MIXER WITH LOAD CONDUCTANCE AS A PARAMETER

V. REFERENCES

1. F. Arams, E. Sard, B. Peyton, and F. Pace, "Infrared 10.6-Micron Heterodyne Detection with Gigahertz IF Capability," IEEE Journal of Quantum Electronics, Vol QE-3, p 484-492, November 1967.
2. F. Arams, B. Peyton, F. Pace, and R. Lange, "Packaged Infrared 10.6-Micron Heterodyne 1-GHz Bandwidth Receiver," presented at Electron Devices Meeting, Washington, D. C., October 1968, to be published.
3. S. Silver, Microwave Antenna Theory and Design, MIT Radiation Laboratory Series, Vol 12, Chapter 6, McGraw-Hill, New York, 1949.
4. G. W. Stroke, "Diffraction Gratings," Handbuch der Physik, S Flugge, ed., Vol XXIX, Springer, Berlin, 1968.
5. B. Richards and E. Wolf, "Electromagnetic Diffraction in Optical Systems II. Structures of the Image Field in a Aplanatic System," Proc Royal Society (London), Vol A253, p 358-379, 1959.
6. D. J. Innes and A. L. Bloom, Spectra-Physic Laser Technical Bulletin No. 5, Spectra-Physics Inc., Mountain View, California, 1966.
7. G. A. Korn and T. A. Korn, Mathematical Handbooks for Scientists and Engineers, Section 21.8, McGraw-Hill, New York, 1961.
8. M. Born and E. Wolf, Principles of Optics, Second Edition, Chapter 8, Macmillan Co., New York, 1964.
9. J. F. Ramsey, "Fourier Transforms in Aerial Theory, Part V, FourierApproximation Curves," Vol X, p 157-165, Marconi Review, 1947.
10. E. Snitzer, "Cylindrical Dielectric Waveguide Modes," and E. Snitzer and H. Osterberg, "Observed Dielectric Waveguide Modes in the Visible Spectrum," Journal of the Optical Society of America, Vol 51, p 491-505, May 1961.
11. N. S. Kapany and R. J. Simms," Fibre Optics, XI, Infrared Region," presented at Optical Society of America Spring Meeting, Washington, D. C., 1964.
12. R. A. Soref, "Extrinsic Infrared Photoconductivity of Si Doped with B, Al, Ga, As, or Sb," Journal of Applied Physics, December 1967.
13. M. DiDomenico and O. Svelto, "Solid-State Photodetection: A Comparison between Photodiodes and Photoconductors," Proc IEEE, February 1959.
14. G. Lucovsky, M. E. Lasser, and R. B. Emmons, "Coherent Light Detection in Solid-State Photodiodes," Proc IEEE, Vol 51, p 166, January 1963.
15. L. K. Anderson, "Measurement of the Microwave Modulation Frequency Response of Junction Photodiodes," Proc IEEE, May 1963.

BLANK PAGE

APPENDIX
MICROWAVE ANTENNA APPROACH TO MIXER ARRAY DESIGN*

1. OPTIMUM SIZE OF A SINGLE MIXER AT A FOCUS

Consider a mixer placed at the focus of a convergent lens upon which a plane wave is incident. The mixer is assumed to be a square, of side a; to simplify the analysis, the lens is also assumed to be square, of side A. A Cartesian coordinate system is set up at the focus, with the z axis aligned with the axis of the lens. The focal length is f, and the F-number is: $F = f/A$.

The diffraction pattern, in the focal plane, at wavelength λ is given in electric field strength by:

$$E(x, y) = E_1(x)\, E_2(y) = \frac{\sin(\pi Ax/\lambda f)}{\pi Ax/\lambda f} \cdot \frac{\sin/\pi Ay/\lambda f}{\pi Ay/\lambda f}$$

$$= \operatorname{sinc}\left(\frac{\pi Ax}{\lambda f}\right) \operatorname{sinc}\left(\frac{\pi Ay}{\lambda f}\right)$$

where

$$\operatorname{sinc} x = \frac{\sin x}{x}$$

The central focal spot is approximately circular at the -3 db level, but has a square periphery where the field is zero. The major sidelobes lie along the x and y axes. Although this focal pattern does not have the circular symmetry of the classical optical focal pattern obtained with a circular objective lens, it is simpler to analyze since the associated functions are trigonometrical, rather than of Bessel type. Also, the square pattern is the product of two separable functions so that only single integrations are required; we can consider the behavior in only one principal plane, where a linear mixer is intercepting a one-dimensional distribution of field of type sinx/x, obtained by taking a section of the solid, or two-dimensional pattern, in the plane of the paper.

The efficiency of the square mixer element, in respect to capture ability, is the ratio of the captured energy to the total energy flowing through the focal plane. As the mixer

---

* The mathematical notation used here is not identical to that used in the main text.

material is phase sensitive, an increase in its width beyond the central spot reduces the mixed output, since the mixer picks up the antiphase field of the first sidelobe region.

The phase sensitive mixer will deliver maximum IF voltage when it receives a plane wave element across its area; that is, when it is uniformly illuminated. At the focal plane, the mixer is not uniformly illuminated because of the shape of the focal diffraction pattern, and because, beyond the central spot there are phase alternations in the sidelobes, (or fringes). To determine the mixer efficiency, it is therefore necessary to determine how it responds to the nonuniform wave represented by the focal diffraction pattern.

Since the mixer is phase sensitive, it picks up the different elements of the wave-front incident upon it and adds them vectorially, providing a summed signal which appears at IF. Thus, the mixer behaves as a small antenna at the focus, and is analogous to a receiving "feed" at a microwave antenna focus. The peak intensity is then, for square lenses:

$$P_1 = \frac{1}{a^2}\left|\int_{-a/2}^{a/2} \operatorname{sinc}\frac{\pi Ax}{\lambda f}\,dx\right|^2 \left|\int_{-a/2}^{a/2} \operatorname{sinc}\frac{\pi Ay}{\lambda f}\,dy\right|^2$$

Where the mixer fully efficient, in the optical sense, it would capture all the power incident on the main objective; that is, all the power in its focal region, by Rayleigh's theorem, or

$$P_2 = \int_{-\infty}^{\infty} \operatorname{sinc}^2\frac{\pi Ax}{\lambda f}\,dx \int_{-\infty}^{\infty} \operatorname{sinc}^2\frac{\pi Ay}{\lambda f}\,dy$$

Hence, the total-power mixer efficiency is the ratio

$$\eta_{\substack{\text{total}\\\text{power}}} = \frac{1}{a^2}\frac{\left|2\int_o^{a/2} \operatorname{sinc}\frac{\pi Ax}{\lambda f}\,dx\right|^4}{\left[2\int_o^{\infty} \operatorname{sinc}^2\frac{\pi Ay}{\lambda f}\,dx\right]^2}$$

$$= \frac{4\lambda^2 f^2}{\pi^2 A^2 a^2}\,\frac{\left[\operatorname{Si}\left(\frac{\pi Aa}{2\lambda f}\right)\right]^4}{(\pi/2)^2}$$

where Si(x) is the sine integral.

Let $k = Aa/2\lambda f$, so that $a = 2kF\lambda$; then

$$\eta_{\substack{\text{total}\\ \text{power}}} = \frac{4}{\pi^2} \frac{\left[\text{Si}(k\pi)\right]^4}{(k\pi)^2}$$

$$= 4k^2 \left[\frac{\text{Si}(k\pi)}{k\pi}\right]^4$$

The value of efficiency is identical with that derived by microwave antenna analysis of the transmitting case where the mixer is replaced by a feed.

Curve 1 in Figure A-1 is a graph of total-power receiving efficiency versus k. A maximum efficiency of 68 percent is obtained when $k = 0.68$. The mixer size is then given by

$$a = 1.36\, F\lambda$$

With $\lambda = 10.6$ microns and $F = 40$, the mixer would be 577-microns square.

We also define a second mixer efficiency, which normalizes the power captured to that in the mainlobe of the airy disk:

$$\eta_{\text{mainlobe}} = \frac{1}{a^2} \frac{\left| 2 \int_0^{a/2} \text{sinc}\, \frac{\pi Ax}{\lambda f}\, dx \right|^4}{\left[2 \int_0^{F\lambda} \text{sinc}\, \frac{\pi ax}{\lambda f}\, dx \right]^2}$$

Curve 2 in Figure A-1 is a graph of mainlobe receiving efficiency. A maximum value of 82 percent is obtained for $k = 0.68$.

If the lens is circular (of diameter D) and the mixer is circular (of diameter a) the optimum mixer diameter is determined by the same method as in the foregoing; only the functions are different. The focal diffraction pattern of the circular lens with a plane wave incident is:

$$E(x) = \frac{\pi D^2}{4\lambda f} \frac{2J_1(\pi x/F\lambda)}{(\pi x/F\lambda)} \qquad F = \frac{f}{D}$$

where x is the radial coordinate in the focal plane.

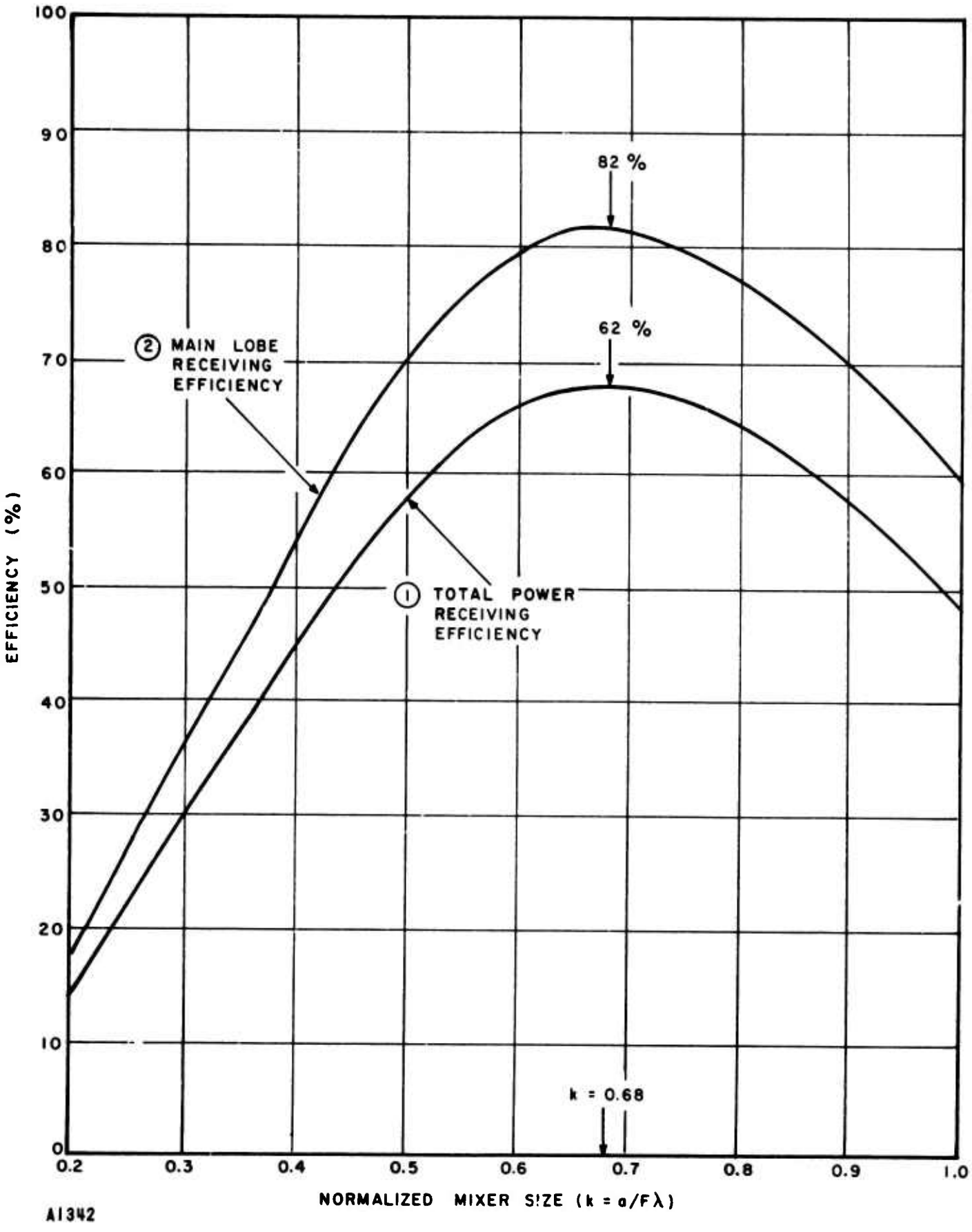

FIGURE A-1. CALCULATED EFFICIENCY VS MIXER SIZE (SQUARE MIXER, SQUARE LENS)

The efficiency is then:

$$\eta_c = \frac{4}{\pi a^2} \left| 2\pi \int_0^{a/2} \frac{\pi D^2}{4\lambda f} \frac{2 J_1(\pi Dx/f\lambda)}{(\pi Dx/f\lambda)} \, x \, dx \right|^2 \frac{4}{\pi D^2}$$

$$= \frac{16}{a^2} \left| \int_0^{a/2} J_1\left(\frac{\pi Dx}{f\lambda}\right) dx \right|^2$$

$$= 4 \frac{4 f^2 \lambda^2}{\pi^2 D^2 a^2} \left[1 - J_o\left(\frac{\pi Da}{2f\lambda}\right) \right]^2$$

Let $k_c = Da/2f\lambda$, then

$$\eta_c = 4 \left[\frac{1 - J_o\left(k_c \pi\right)}{k_c \pi} \right]^2$$

The mixer diameter is then

$$a = 1.7 \, F\lambda$$

and at 10.6 microns, with F = 40, the mixer would have a diameter of 721 microns.

2. SINGLE MIXER OFF-AXIS FOCAL DIFFRACTION PATTERN CENTERED ON-AXIS (TWO MIXERS)

To determine the geometry for a two-dimensional array of mixers in the focal plane, it is first necessary to investigate the response of a single mixer at an off-axis position, when the beam is on-axis. For a mixer of side a, centered a distance (d) off-axis, the received field is:

$$E = \int_{d-a/2}^{d+a/2} \frac{\sin \pi x/F\lambda}{\pi x/F\lambda} \, dx$$

$$= \frac{F\lambda}{\pi} \left\{ Si\left[\frac{\pi}{F\lambda}\left(d + \frac{a}{2}\right)\right] - Si\left[\frac{\pi}{F\lambda}\left(d - \frac{a}{2}\right)\right] \right\}$$

Using $a = 2kF\lambda$, and normalizing the field to the value for $d = 0$,

$$E_n = \frac{\mathrm{Si}\left[\pi\left(k + \frac{d}{F\lambda}\right)\right] + \mathrm{Si}\left[\pi\left(k - \frac{d}{F\lambda}\right)\right]}{2\,\mathrm{Si}(\pi k)}$$

This is the receiving pattern obtained by sliding the mixer across the sin x/x focal pattern; that is, by varying d. Alternatively, this pattern would be obtained by placing the mixer at the focus and rotating the antenna.

If two adjacent mixers are placed one on each side of the axis, without a gap, then the signal received by each mixer has an intensity determined by $d = a/2$, or:

$$E_{co}^2 = \left[\frac{\mathrm{Si}(2k\pi)}{2\,\mathrm{Si}(k\pi)}\right]^2$$

Expressed in decibels, relative to the signal obtained when one mixer is on axis, E_{co}^2 is the "crossover level." For a receiving antenna, the crossover level is the level, relative to either receiving pattern peak, where the incident wave is in the axial direction. In a focused antenna, the axial diffraction pattern at the focus falls midway between two "feeds" (mixers in the present case).

In the diffraction theory of antennas, the generalized angle due to Lommel is πAu. The equivalent generalized off-axis displacement in the focal region is $\pi d/F\lambda$, since:

$$\frac{\pi d}{F\lambda} = \frac{\pi d}{f}\,\frac{A}{\lambda} = \pi A\,\frac{\theta}{\lambda} = \pi Au$$

Generalized focal region data can then be plotted in terms of $d/F\lambda$; this alternative form having been used by Rayleigh.

The focused diffraction pattern produced by an axial plane wave is:

$$E_f = \frac{\sin(\pi x/F\lambda)}{\pi x/F\lambda}$$

and would be measurable by an infinitesimal-field probe taken across the focal plane. When a mixer of finite area moves across the focal plane it receives an integrated contribution at each point, given by:

$$E_n = \frac{\mathrm{Si}\left[\pi\left(k + \frac{d}{F\lambda}\right)\right] + \mathrm{Si}\left[\pi\left(k - \frac{d}{F\lambda}\right)\right]}{2\,\mathrm{Si}(k\pi)}$$

In Section I, it was found that k = 0.68 maximized the receiving efficiency. When a mixer having a = 1.36 Fλ is moved across the focal plane, the focal reception pattern, as it may be called, is E_n, with k = 0.68. The difference between this pattern and the focused diffraction pattern (E_f) is shown in Figure A-2. It is observed that the receiving pattern is broader than the focal pattern, and that the sidelobes are reduced. The focal plane receiving pattern, with the optimum mixer, is identical with the far-field pattern in space of the objective and mixer, regarded as an antenna system. Thus, sliding the mixer through the focus is a convenient way of determining the antenna beamwidth and sidelobes without movement of the antenna.

If the receiving patterns for different values of k are plotted, the 3-db width of the patterns can be expressed in terms of k (as in Figure A-3). These widths are also the beamwidths of the secondary radiation patterns from the objective on the far field. For if d_0 is the off-axis distance at which the level of the receiving pattern is 3 db down from the peak, $2d_0/F\lambda = k$. Say that $2d_0/f\ A/\lambda = k$, but $d_0/f = \theta_0$ in the far field. Hence, the far-field beamwidth is BW = $k\ \lambda/A$ radians.

3. TWO MIXERS SEPARATED BY A GAP

When mixers are arrayed, gaps are necessary for constructional purposes. In the simplest case two mixers, of side a each, can be taken with a center-to-center spacing, s. The spacing can be normalized to the width by letting

$$\sigma = \frac{s}{a} \quad \text{or} \quad s = \sigma a$$

The receiving pattern of a mixer, say at the focus, is the function of x given by:

$$E_n(x) = \frac{\mathrm{Si}\left[\pi(k + x/F\lambda)\right] + \mathrm{Si}\left[\pi(k - x/F\lambda)\right]}{2\ \mathrm{Si}(k\pi)}$$

At the crossover, $x = s/2 = 1/2\sigma a$, hence

$$E_n(s/2) = \frac{\mathrm{Si}\left[\pi(k + \sigma a/2F\lambda)\right] + \mathrm{Si}\left[\pi(k - \sigma a/2F\lambda)\right]}{2\ \mathrm{Si}(k\pi)}$$

$$= \frac{\mathrm{Si}\left[\pi k(1 + \sigma)\right] + \mathrm{Si}\left[\pi k(1 - \sigma)\right]}{2\ \mathrm{Si}(k\pi)}$$

since

$$k = \frac{a}{2F\lambda}$$

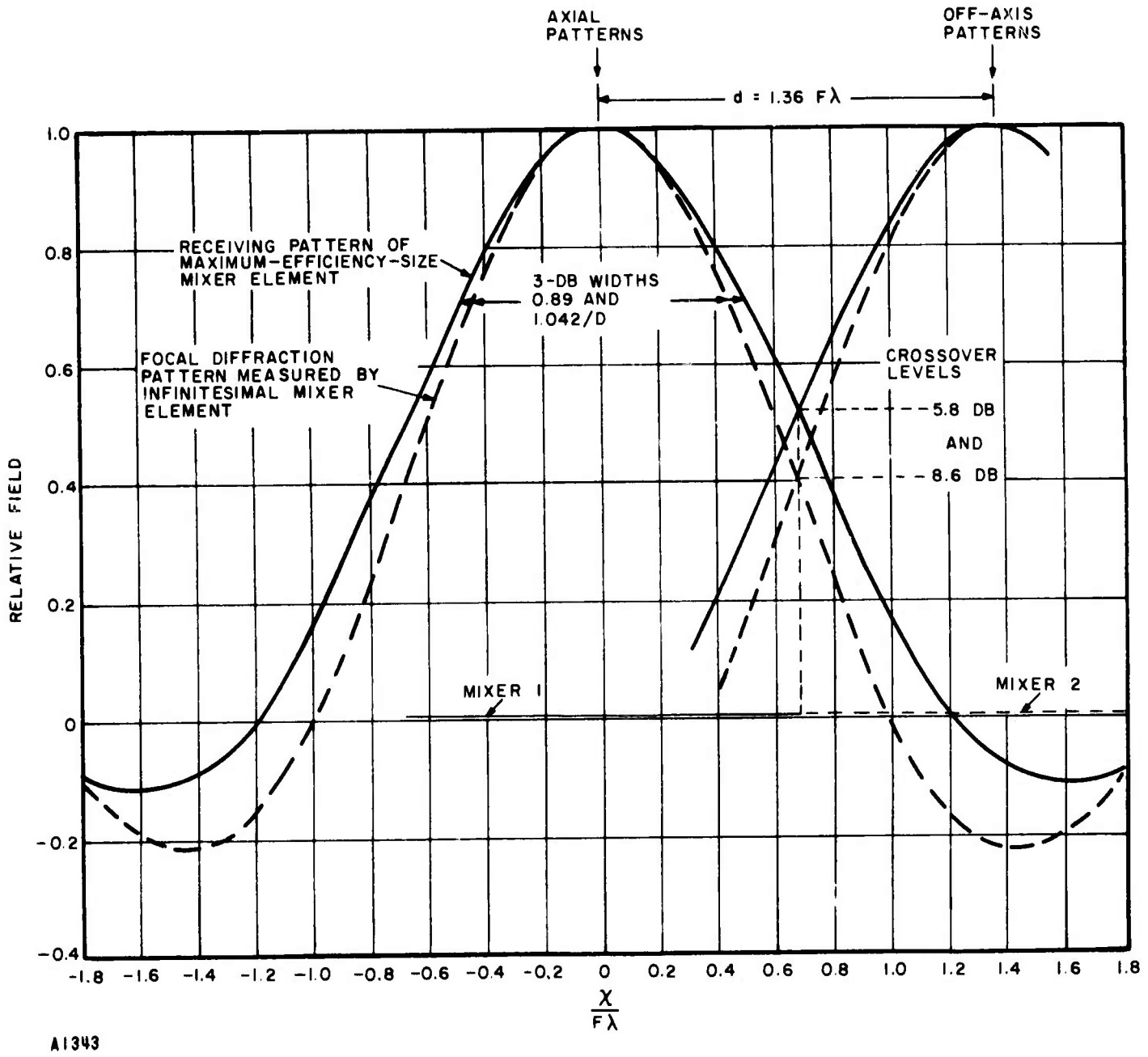

FIGURE A-2. COMPARISON BETWEEN FOCAL PATTERNS MEASURED BY AN INFINITESIMAL MIXER AND BY A MAXIMUM EFFICIENCY-SIZE MIXER (SQUARE OBJECTIVE, SQUARE MIXERS)

The variation of the crossover level with a and s can be plotted in terms of k, with σ as a parameter as shown in Figure A-4. The efficiency, which is not affected by s unless there is mutual coupling, is shown as a function of k below the crossover family (for a square objective and square mixer elements).

Figure A-4 also shows the crossover levels and efficiency for a circular objective and square mixer elements for $\sigma = 1$. The beamwidths of a circular objective are broader than that of a square objective, so that the crossover levels are higher for a given mixer size.

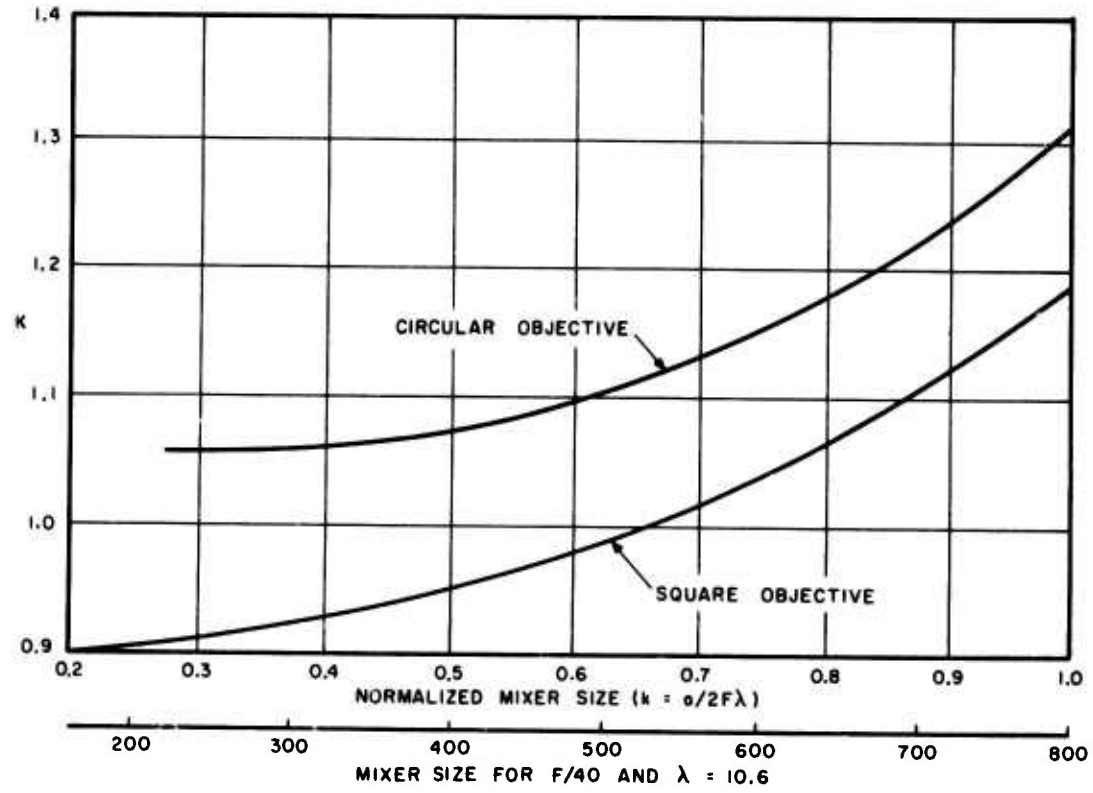

FIGURE A-3. BEAMWIDTHS OF FAR-FIELD PATTERNS VS MIXER SIZE (SQUARE MIXER)

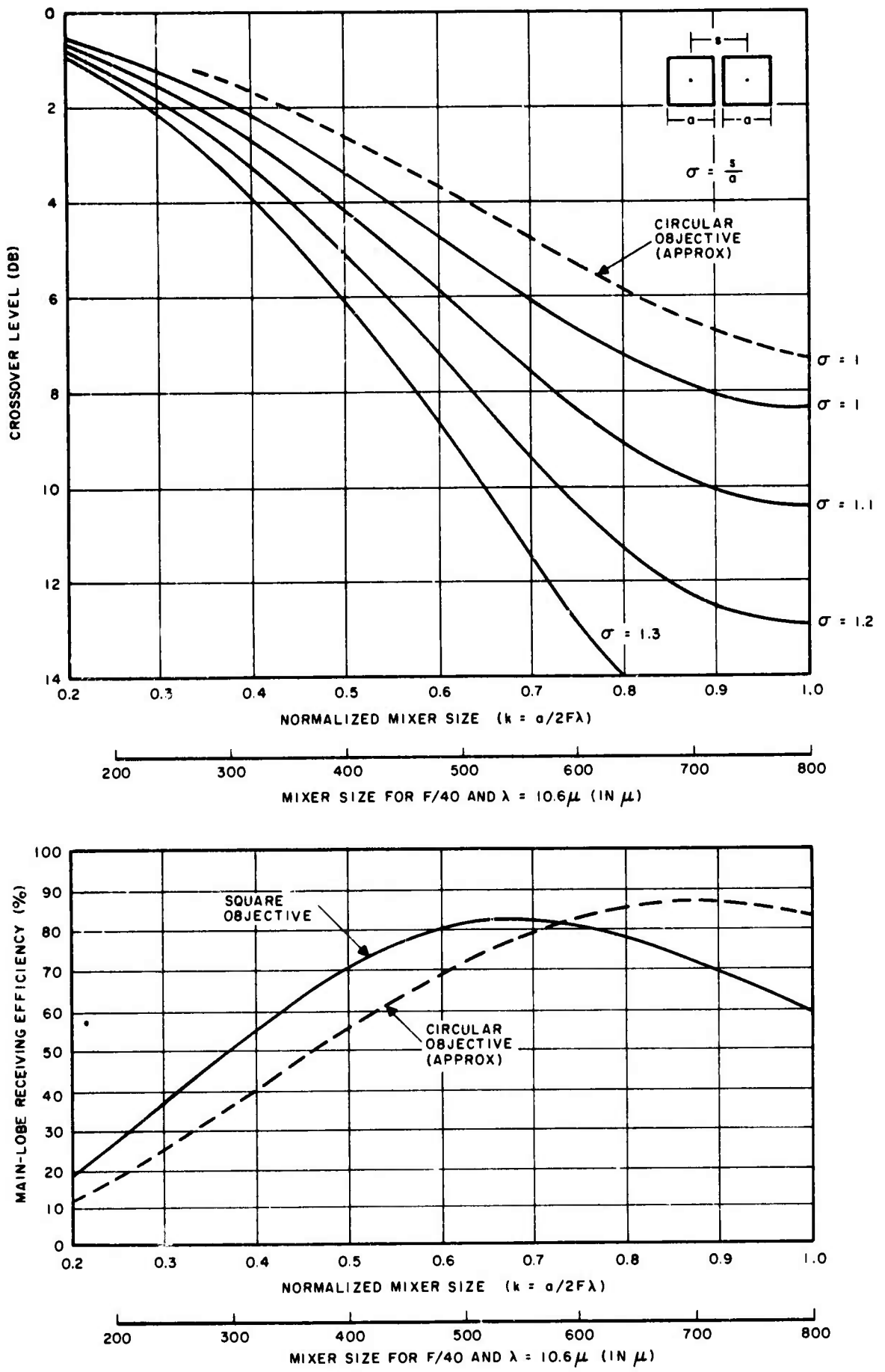

FIGURE A-4. CROSSOVER LEVEL AND EFFICIENCY VS MIXER SIZE (SQUARE MIXER)

UNCLASSIFIED

Security Classification

DOCUMENT CONTROL DATA - R & D

(Security classification of title, body of abstract and indexing annotation must be entered when the overall report is classified)

1. ORIGINATING ACTIVITY *(Corporate author)*
AIRBORNE INSTRUMENTS LABORATORY
A DIVISION OF CUTLER-HAMMER, INC.
Deer Park, New York 11729

2a. REPORT SECURITY CLASSIFICATION
UNCLASSIFIED

2b. GROUP

3. REPORT TITLE
ADVANCED CAPABILITY INFRARED RECEIVER SYSTEM

4. DESCRIPTIVE NOTES *(Type of report and inclusive dates)*
First Semiannual Progress Report (15 March 1968 to 15 September 1968)

5. AUTHOR(S) *(First name, middle initial, last name)*
F. Pace, F. Arams, R. Lange, B. Peyton, E. Sard, and J. Ramsey

6. REPORT DATE	7a. TOTAL NO. OF PAGES	7b. NO. OF REFS
October 1968	75	15

8a. CONTRACT OR GRANT NO.	9a. ORIGINATOR'S REPORT NUMBER(S)
N00014-68-C-0273	AIL Report 3481-I-1
b. PROJECT NO. 7E20K21	
c. ARPA Order No. 306	9b. OTHER REPORT NO(S) *(Any other numbers that may be assigned this report)*
d.	

10. DISTRIBUTION STATEMENT
Reproduction in whole, or in part, is permitted for any purpose of the United States Government.

11. SUPPLEMENTARY NOTES	12. SPONSORING MILITARY ACTIVITY
This research is part of Project DEFENDER under the joint sponsorship of the Advanced Research Project Agency, the Office of Naval Research, and the DOD.	Office of Naval Research

13. ABSTRACT
This is the First Semiannual Report on a program to demonstrate the feasibility of a 10.6-micron coherent receiver array with 1.5-GHz IF bandwidth, 3 X 3 elements with -3 db antenna-beam crossovers, and near quantum-noise limited sensitivity. The two primary areas of investigation were: (1) coherent array development, which includes the formulation of an analytical model of a coherent multiple-beam array, computer-generated antenna patterns, laboratory verification of these patterns, and formulation of diffraction-limited image dissection techniques, and (2) mixer development, which included achieving Ge:Cu mixer response to 1.43 GHz (with NEP equal to, or less than, 1.5×10^{-19} Hz/watt over this band), analysis of wideband photovoltaic mixing, measurements of 9 mixers of various types, and continued development of a single amplifier to cover the band from 10 MHz to 1.5 GHz.

DD FORM 1 NOV 65 1473

UNCLASSIFIED

Security Classification

14. KEY WORDS	LINK A		LINK B		LINK C	
	ROLE	WT	ROLE	WT	ROLE	WT
Antenna Patterns						
Coherent Array						
CO_2 Lasers						
Infrared Mixer						
Photovoltaic Mixer						
10.6 Micron Mixer						